

OmniFaceRig: Fully Automatic Inner-Mouth-Aware Face Rigging Across Diverse 3D Character Topologies

Chao Wang^{*,†,‡}, Guangyao Ma^{*}, John Doublestein, Junming Chen, Yiming Lin, Zhaoen Su, Xiaomin Luo, Shiyang Cheng, Jie Shen, Doug Roble, Dilin Wang, Yilei Li[†], Rakesh Ranjan[†]

Reality Labs, Meta

*Equal contribution, †Project lead, ‡Corresponding author

Facial rigging—creating FACS-based blendshapes together with inner-mouth geometry (teeth, gums, and tongue)—remains a major bottleneck in 3D character production. Existing pipelines still require substantial designer effort, especially for manual landmark annotation, per-character template adjustment, and inner-mouth placement. We present **OmniFaceRig**, a fully automatic end-to-end pipeline that converts a static surface-only 3D character mesh, with no pre-modeled oral cavity, into an inner-mouth-aware FACS rig with up to 155 blendshapes, procedurally fitted teeth, gums, and tongue, and re-packed UV/texture. OmniFaceRig supports diverse topologies—humans, humanoids, long-muzzled animals (e.g., dogs, wolves, foxes), and short-muzzled animals (e.g., cats, bears, rabbits, tigers)—with no manual landmarks, no user-provided templates, and no per-asset setup. The pipeline combines hybrid VLM+CV riggability checking, multi-model face parsing, dense keypoint-driven template registration, procedural inner-mouth construction, and collision-aware blendshape transfer. For non-human characters, OmniFaceRig selects topology-specific face and inner-mouth templates and uses collision-aware inner-mouth fitting to reduce teeth-face intersections without exposing users to category-specific tuning. We also publicly release **Omni-Bench**, a freely available benchmark dataset of 1,000 biped 3D characters with FACS facial blendshapes and inner-mouth geometry, spanning humans, humanoids, cats, dogs, and other animals. Experiments show high final rigging success on screened Omni-Bench inputs, nearly complete face detection recall from the segmentation ensemble, reliable inner-mouth placement with low penetration, and 20–30s end-to-end processing time per asset on a single A100 GPU, including data I/O. Together, OmniFaceRig provides an automatic path from static generated characters to animation-ready facial rigs across both human and non-human topologies.

Date: June 9, 2026

Project page and dataset: <https://omnifacerig.github.io>



Contents

1	Introduction	2
2	Omni-Bench: Benchmark Dataset	3
3	OmniFaceRig Method	5
3.1	Pipeline Overview	5
3.2	Riggability Assessment	5
3.3	Sapiens-Based Segmentation Models	9
3.4	Face Detection and Segmentation	9
3.5	Template Registration	10
3.6	Blendshape Rig Construction	13
4	Experiments	15

4.1	Setup	15
4.2	Implementation Details	15
4.3	Evaluation Metrics and Baselines	18
4.4	Quantitative Results	18
4.5	Ablation Studies	19
4.6	Latency Breakdown	20
5	Related Work	21
5.1	3D Asset and Character Generation	21
5.2	Parametric Face Models vs. Blendshape Rigging	21
5.3	Traditional and Learning-Based Facial Auto-Rigging	22
5.4	Neural Face Avatars	23
5.5	Rigging for Non-Humanoid Characters	23
6	Conclusions and Limitations	24
A	Additional Qualitative Results	30

1 Introduction

Facial rigging—creating FACS-based blendshapes and inner-mouth geometry (teeth, gums, and tongue) for 3D character animation—remains one of the most labor-intensive steps in the character production pipeline. A skilled technical artist may spend hours to days sculpting blendshapes for a single character, involving careful topology design, facial landmark placement, expression sculpting, and teeth fitting.

At the same time, 3D asset creation itself has become dramatically more accessible. Recent text-to-3D and image-to-3D methods can generate textured objects or characters directly from prompts or reference images (Poole et al., 2023; Lin et al., 2023; Jun and Nichol, 2023; Liu et al., 2023; Tang et al., 2024; Ren et al., 2023), including high-quality asset-generation systems such as Meta 3D AssetGen (Siddiqui et al., 2024) and its follow-on AssetGen2 model (Ranjan et al., 2025). However, these systems primarily produce static surface meshes and textures. For characters, the generated assets are often plausible as visual meshes but are not animation-ready facial rigs: they typically lack FACS controls, robust facial topology for deformation, and the oral-cavity geometry required for inner-mouth-aware expressions. This makes generated characters natural inputs to an automatic rigging pipeline, but not substitutes for such a pipeline.

Existing rigging solutions address parts of this problem but remain incomplete and, in practice, only *semi-automatic*. Deformation transfer (Sumner and Popović, 2004) and parametric face models (Cao et al., 2014; Li et al., 2017) enable facial rig creation but assume compatible mesh topologies, require manual landmark annotation, and are designed primarily for human faces. Inner-mouth geometry (teeth, gums, and tongue) is particularly costly to author because the input mesh normally contains no corresponding interior surfaces: in production pipelines, teeth, gums, and tongue are typically placed and tuned by hand, and manually tuned or human-specific teeth templates often fail on stylized or non-human faces. We are not aware of a prior fully automatic, end-to-end pipeline that produces FACS blendshapes with newly generated inner-mouth geometry from a static surface-only mesh, especially across both human and non-human topologies.

We present **OmniFaceRig**, an end-to-end pipeline for face auto-rigging across diverse 3D character topologies—including humans, humanoids, long-muzzled animals (e.g., dogs, wolves, foxes), and short-muzzled animals (e.g., cats, bears, rabbits, tigers). These animal labels describe coarse facial topology for template selection rather than biological taxonomy: long-muzzled characters have elongated, forward-protruding snouts, while short-muzzled characters have compact or nearly absent snouts. Given a static surface-only 3D mesh with no pre-modeled oral cavity, OmniFaceRig produces a production-ready facial rig with up to 155 FACS blendshapes, procedurally generated inner-mouth geometry (teeth, gums, and tongue), and re-packed UV/-texture, all fully automatic with no manual intervention at any stage. In particular, OmniFaceRig eliminates the manual inner-mouth placement, landmark annotation, user-provided templates, and per-asset template setup that bottleneck prior pipelines, allowing the entire facial rig to be generated directly from the input mesh. Our key contributions are:

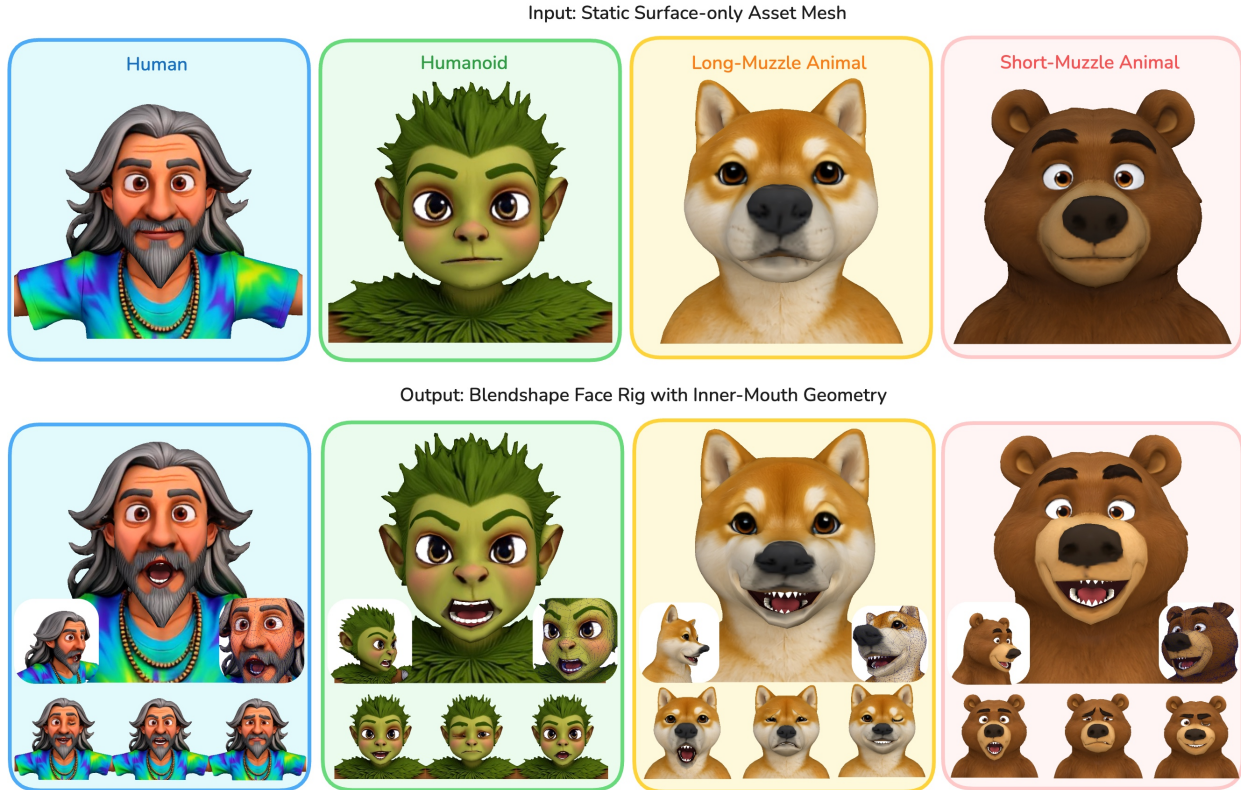


Figure 1 OmniFaceRig takes static surface-only 3D meshes with no pre-modeled oral cavity (top row) and fully automatically produces production-ready facial rigs with FACS blendshapes and generated inner-mouth geometry including teeth, gums, and tongue (bottom rows showing expressions and mouth details). The teaser highlights our support for diverse 3D character topologies—humans, humanoids, long-muzzled animals (e.g., dogs), and short-muzzled animals (e.g., bears)—within one unified rigging pipeline. Omni-Bench is released as a freely available benchmark of rigged biped characters spanning humans and animals.

1. **Fully automatic, end-to-end face auto-rigging pipeline.** OmniFaceRig starts from a static surface-only input mesh and requires no manual inner-mouth placement, landmark annotation, user-provided templates, or per-asset template setup.
2. **Inner-mouth-aware rig construction.** OmniFaceRig procedurally generates teeth, gums, tongue, and oral-cavity support geometry that are absent from the input mesh, then integrates them with FACS blendshape transfer using ARAP+SDF fitting and collision-aware deformation.
3. **Omni-Bench.** We publicly release a benchmark dataset of 1,000 biped 3D characters with FACS facial blendshapes and inner-mouth geometry (teeth, gums, and tongue), spanning humans (realistic + humanoid, 13 occupations), cats (10 breeds), and dogs (10 breeds) with up to 12 appearance variations—all in T-pose and all rigged by OmniFaceRig.
4. **Generalization across diverse non-human topologies.** Our method rigs long-muzzled animals (dogs, wolves, foxes, etc.) and short-muzzled animals (cats, bears, rabbits, tigers, etc.) via a small library of topology-specific templates with a nose-landmark-free design and ARAP+SDF teeth placement, demonstrating that the same pipeline transfers from humans to animals without architectural changes.

2 Omni-Bench: Benchmark Dataset

To facilitate future research in automatic facial rigging, we make Omni-Bench publicly available as a benchmark dataset of biped 3D characters with FACS facial blendshapes and inner-mouth geometry (teeth, gums,

Table 1 Comparison of 3D facial and character datasets. To our knowledge, Omni-Bench is the first dataset providing FACS blendshapes with inner-mouth geometry (teeth, gums, and tongue) for both human and animal full-character assets, along with AssetGen2-style text/image-to-3D generation pipeline data.

Dataset	Year	Total Models	Species	FACS Blendshapes	Inner Mouth	Full Character	Text + 2D Image
BFM (Paysan et al., 2009)	2009	200	Human	✗	✗	✗	✗
CoMA (Ranjan et al., 2018)	2018	144	Human	✗	✗	✗	✗
VOCASET (Cudeiro et al., 2019)	2019	12 (4D)	Human	✗	✗	✗	✗
FaceScape (Zhu et al., 2023)	2020	16,940	Human	✗	✗	✗	✗
ICT FaceKit (Li et al., 2020b)	2020	1 (Parametric)	Human	✓	✓	✗	✗
Multiface (Wuu et al., 2022)	2022	13 (Multi-view)	Human	✗	✗	✗	✗
RaBit (Luo et al., 2023)	2023	1,500	Human & Cartoon	✗	✗	✓	✗
Anymate (Deng et al., 2025)	2025	230,000	Human & Animal	✗	✗	✓	✗
Omni-Bench (Ours)	2026	1,000	Human & Animal	✓	✓	✓	✓

and tongue). The initial static character meshes are produced with a variant of AssetGen2 (Ranjan et al., 2025), a follow-on model in the Meta 3D AssetGen family (Siddiqui et al., 2024); all released assets are then selected from inputs that pass the initial VLM+CV riggability screen, are processed by OmniFaceRig, and are provided in biped T-pose with generated rig outputs.

The development of robust facial rigging algorithms relies heavily on high-quality 3D datasets. Early datasets like BFM (Paysan et al., 2009) provided PCA-based morphable models but lacked diverse expressions. FaceScape (Zhu et al., 2023; Yang et al., 2020) significantly advanced the field with 16,940 topologically uniform models, though it only captures the outer facial surface. Multiface (Wuu et al., 2022) and VOCASET (Cudeiro et al., 2019) provide high-quality scans for neural rendering and speech-driven animation, but do not provide FACS blendshape rigs. ICT FaceKit (Li et al., 2020b) offers a detailed morphable model including teeth, gums, and eyes, but as a single parametric model rather than a diverse dataset. Existing large-scale character datasets such as RaBit (Luo et al., 2023) and Anymate (Deng et al., 2025) provide many full-character assets, but they do not include FACS facial blendshapes or inner-mouth structures.

Omni-Bench addresses these gaps with 1,000 rigged biped 3D characters, split into 500 human and humanoid characters and 500 animals. The human set covers realistic humans across 13 common occupations (astronaut, doctor, firefighter, soldier, chef, pilot, nurse, teacher, police officer, engineer, athlete, musician, scientist) as well as stylized humanoid characters (fantasy, sci-fi, and cyberpunk styles). The animal set is dominated by 150 cats (10 breeds: Persian, Siamese, Maine Coon, Sphynx, Ragdoll, British Shorthair, Bengal, Abyssinian, Scottish Fold, Russian Blue) and 150 dogs (10 breeds: Husky, Pug, Labrador, German Shepherd, Corgi, Poodle, Golden Retriever, Bulldog, Beagle, Dalmatian), plus 200 other common animals amenable to rigging (e.g., bears, mice, tigers, lions, foxes, wolves, rabbits, deer); all of them are provided in biped form like the rest of Omni-Bench. Categories include up to 12 appearance variations. Figure 4 provides a visual overview of the dataset diversity and topology coverage.

The riggability screen should be interpreted as an input eligibility filter rather than a guarantee of final rigging success. It removes obvious invalid assets—for example, missing faces, severe eye or mouth occlusions, non-standard viewpoints, or unsupported facial topologies—before full processing. A screened asset can still fail during later stages because of segmentation errors, unstable template fitting, or implausible mouth localization. We therefore report final *Success Rate* separately in the experiments as the percentage of screened Omni-Bench inputs for which the full OmniFaceRig pipeline completes and passes final geometric quality checks.

As shown in Table 1, Omni-Bench stands out in three critical ways. First, it supports both human and animal characters within a unified rigging framework. Second, every model is equipped with a complete set of auto-generated FACS blendshapes (up to 155 shapes) that explicitly include teeth, gums, and tongue—a feature missing from most existing large-scale character datasets. Third, each asset includes the complete generation pipeline data: the initial text description, intermediate 2D reference image, and final AssetGen2-generated 3D mesh, making it a useful resource for text-to-3D generation (Siddiqui et al., 2024; Ranjan et al., 2025; Tang et al., 2024; Ren et al., 2023) and multimodal research. All assets are in biped T-pose and rigged by OmniFaceRig, providing a consistent and reproducible evaluation baseline.

Table 2 Comparison of facial auto-rigging methods. OmniFaceRig is the only compared method achieving fully automatic blendshape generation with no per-asset setup, supporting disconnected components including inner-mouth geometry (teeth, gums, and tongue), and generalizing across diverse human and animal character topologies. “No Per-Asset Setup” means no user-provided template, manual landmarking, or per-character fitting adjustment at inference time.

Method	Cross-Topology	No Manual Landmarks	No Per-Asset Setup	Output Format	Disconnected Parts	Inner Mouth	Animal Support
Deformation Transfer (Sumner and Popović, 2004)	✗	✗	✗	Mesh	✗	✗	✗
Example-Based (Li et al., 2010)	✗	✗	✗	Blendshapes	✗	✗	✗
Li et al. (Li et al., 2020a)	✗	✗	✗	Blendshapes	✗	✗	✗
Chandran et al. (Chandran et al., 2022b)	✓	✗	✗	Mesh	✗	✗	✗
NFR (Qin et al., 2023)	✓	✓	✓	Mesh / Latent	✗	✗	✗
NFDI (Chandran et al., 2025)	✓	✓	✓	Blendshapes	✗	✗	Limited
NFS (Cha et al., 2025)	✓	✓	✓	Skinning Weights	✓	✗	✗
RigAnyFace (Ma et al., 2025)	✓	✓	✓	Blendshapes	✓	✗	✗
OmniFaceRig (Ours)	✓	✓	✓	Blendshapes	✓	✓	✓

3 OmniFaceRig Method

Before presenting the OmniFaceRig pipeline in detail, we position our system against prior facial auto-rigging work along the dimensions that matter most for production deployment: topology coverage, the need for manual landmarks or per-asset setup, the output rig format, support for disconnected components, inclusion of inner-mouth geometry, and animal generalization. Table 2 summarizes this comparison; among the compared methods, OmniFaceRig is the only one that satisfies all six criteria simultaneously, in particular adding fully procedural inner-mouth construction (teeth, gums, and tongue) and non-humanoid character support on top of the strongest existing learning-based pipelines. The rest of §3 describes how each of these properties is realized; §5 discusses the individual prior systems referenced in the table.

3.1 Pipeline Overview

OmniFaceRig takes a static surface-only 3D mesh with no pre-modeled oral cavity and produces a production-ready facial rig with FACS blendshapes and inner-mouth geometry (teeth, gums, and tongue) (Figure 2). The pipeline is organized into two stages. Stage 1 (Face Template Fitting) (§3.2–§3.5) lifts the input mesh into a canonical template space through a sequence of steps: we first render the input 3D mesh to a frontal-view character image, then perform face detection and cropping to localize the face region; the cropped face is parsed by a multi-model segmentation ensemble; a hybrid VLM+CV riggability assessment uses visual-semantic predictions together with CV segmentation signals to decide whether to proceed and to select the face/teeth template configuration; 2D and 3D keypoints are extracted from the final segmentation masks; and finally a rigid + non-rigid template registration aligns a canonical face template to the input face, producing a fitted face mesh. Stage 2 (Blendshape Rig Construction) (§3.6) takes the fitted template and constructs a production-ready FACS blendshape rig—fusing the fitted face with the original asset, procedurally generating and placing inner-mouth geometry (teeth, gums, and tongue), baking texture into a re-packed UV layout, and transferring blendshape deformations from a canonical rigged template to the asset.

3.2 Riggability Assessment

Before processing an asset through the rigging pipeline, OmniFaceRig performs an automatic eligibility check. This is critical in production settings where input assets are generated automatically (e.g., from text-to-3D models) and may include characters with no visible face, heavily occluded facial features, non-standard orientations, or facial topologies outside the current template library.

Our riggability assessment is a VLM+CV hybrid that fuses three complementary signals computed from a single frontal render of the input asset: (i) a high-level VLM semantic check, (ii) a set of CV segmentation-mask checks, and (iii) a mouth-landmark quality gate used for human-like inputs. The three signals are summarized below at the level needed for the main pipeline; §3.2.1–§3.2.2 list the full per-question signal assignment and the geometric thresholds applied to each segmentation mask.

VLM Understanding. We render the input 3D mesh from a frontal viewpoint and query a state-of-the-art Vision-Language Model (VLM) to identify: (1) the *character archetype* (human, humanoid, feline, canine,

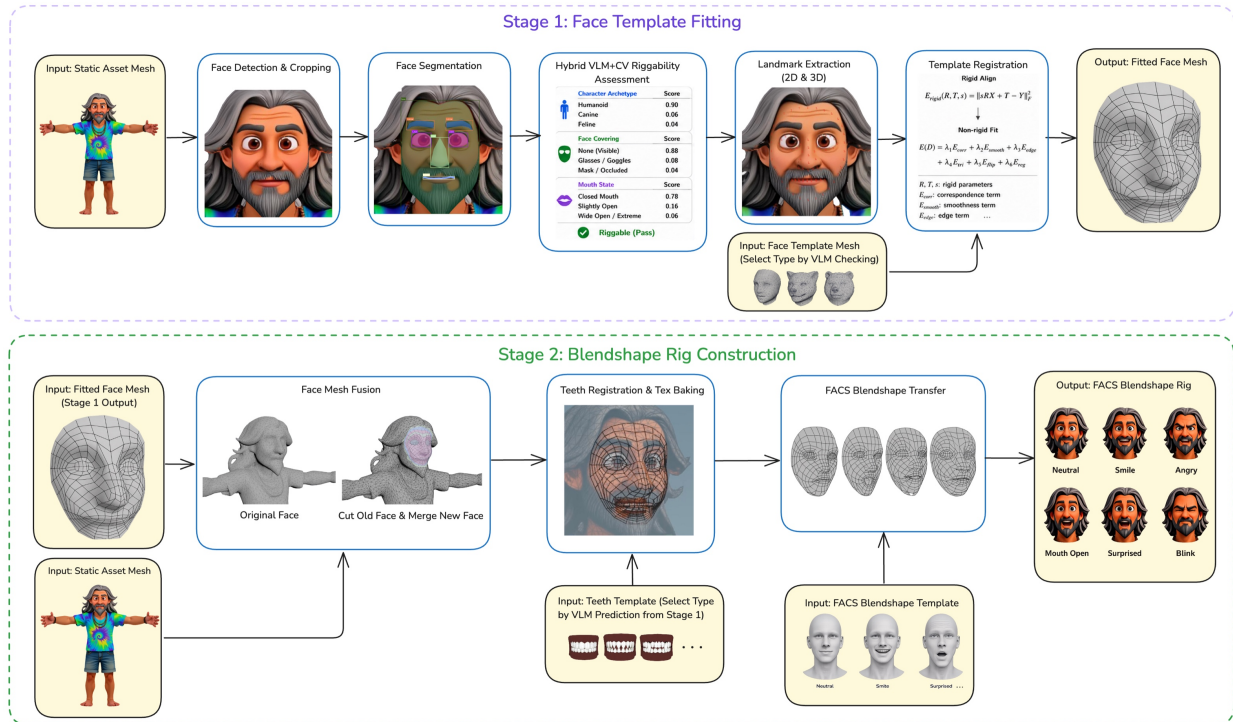


Figure 2 OmniFaceRig pipeline architecture. The pipeline consists of two stages. Stage 1 (Face Template Fitting) takes a static surface-only 3D mesh, performs face detection/cropping, face segmentation, VLM+CV riggability assessment, landmark extraction, and dense keypoint-driven rigid + non-rigid template registration, producing a fitted template mesh aligned to the input face. Stage 2 (Blendshape Rig Construction) takes the fitted template and constructs a production-ready FACS blendshape rig through face mesh fusion, generated teeth registration and texture baking, and FACS blendshape transfer, producing inner-mouth geometry (teeth, gums, and tongue) and re-packed UV/texture that are not present in the input.

or other); (2) *face covering status* (glasses, goggles, masks, eye patches); and (3) *teeth state* (open mouth, closed mouth, emotional expression). The VLM’s flexibility allows easy adaptation to new assessment criteria without retraining. The VLM has two roles. First, it filters out assets that are unlikely to be riggable by the current system, including no-face assets, faces with severe eye or mouth occlusion, and unsupported facial topologies such as highly exaggerated beaked birds or other shapes outside our human, long-muzzle, and short-muzzle template families. Second, for assets that pass this eligibility check, it selects downstream configuration choices: (i) the *face template variant*—one of *human*, *long-muzzle*, or *short-muzzle*—based on the character’s facial topology (see §3.5); and (ii) the *inner-mouth archetype* (human, canine, monster, or flat), which Stage 2 (§3.6) uses for inner-mouth fitting.

CV Segmentation Filtering. After face/eye/mouth segmentation masks using the multi-model ensemble described in §3.4 and apply a layered set of geometric checks. The first layer is an eligibility filter: assets where no valid face region is detected, or where the face area falls below a minimum threshold, are rejected. This catches cases where the VLM may be overconfident—for example, detecting a “face” on a purely mechanical character with no actual facial geometry. The second layer is a set of region-level criteria evaluated on the segmentation masks themselves—eye-region occlusion, eye-to-head size ratio, lip-seal curvature, and mask inclusion—each producing a binary pass/fail signal that participates in the hybrid decision. The full criterion list and the per-region thresholds are given in §3.2.2 (Table 5).

Mouth-Landmark Quality Gate. For human-like inputs, the mouth-landmark signal from the segmentation ensemble is the most accurate way to verify that the mouth is well-formed, but it degrades silently on stylized or non-human characters where the landmark detector still emits points along an ill-defined contour. We therefore gate the landmark mouth evidence by a single lip-evenness statistic (§3.2.1) before it is allowed to influence the mouth decision; for non-human inputs the landmark signal is dropped entirely. This gate is

Table 3 Riggability assessment accuracy on a mixed validation set of approximately 500 assets with human ground-truth riggability labels. The hybrid VLM+CV approach achieves the best performance.

Method	Accuracy	Recall	F1
VLM only	94.69%	94.76%	94.71%
CV segmentation filtering only	76.72%	94.87%	80.87%
VLM + CV (Ours)	>95%	>95%	>95%

the third signal source in our checker.

Hybrid Decision. The final eligibility decision is the conjunction of all per-question results from the three signals above: VLM for high-level semantic checks, segmentation masks for geometric criteria, and—for the mouth-detection question on human-like inputs—an explicit three-way vote combining VLM, segmentation, and landmark evidence (full fusion logic in §3.2.1). We evaluate the hybrid approach on a mixed riggability validation set of approximately 500 assets, including Omni-Bench candidates, a subset of a separate benchmark collection, and additional generated or collected examples. This validation set intentionally includes both riggable and non-riggable inputs; metrics compare the automatic checker decision against human ground-truth riggability labels:

The hybrid approach leverages the VLM’s strong image understanding for high-level decisions while using CV signals for geometric validation, consistently outperforming either component alone.

3.2.1 VLM+CV Signal Architecture

Recall from §3.2 that the checker fuses three signals computed from a single frontal render. This section gives their precise definitions and the per-question assignment used by the fusion logic:

- **VLM semantic signal.** A state-of-the-art Vision-Language Model answers a fixed set of high-level questions about the rendered character (face type, number of faces, eye orbits, accessories, mouth state, teeth visibility). These questions capture failure modes that are inherently semantic and hard to phrase as geometric thresholds.
- **Segmentation-mask signal.** The face/eye/mouth masks produced by the segmentation ensemble (§3.4) are evaluated against geometric plausibility criteria: presence of each region, inclusion inside the face boundary, plausible eye-to-head ratio, and acceptable lip-seal curvature.
- **Landmark-quality signal.** For human-like faces, the regularity of mouth landmarks is summarized by a lip-evenness statistic and used as a quality gate before mouth evidence enters the fusion step.

The three signals are not treated as redundant: each question in the underlying checker template is assigned to the signal that is empirically most reliable for it, as summarized in Table 4.

3.2.2 Geometric Criteria from Segmentation Masks

The segmentation-based checks (Q5, Q9, Q10, plus mask inclusion tests) are summarized in Table 5. The thresholds are calibrated once on a development split and held fixed across all evaluations; they are deliberately conservative so that the checker rejects mostly inputs that would otherwise crash or distort the downstream registration stage.

3.2.3 Landmark-Assisted Mouth Validation

For human-like inputs, we use mouth landmarks as a quality gate before they are fused with the VLM and segmentation signals. Let CV_{lip} denote the coefficient of variation of the spacing between consecutive lip-contour landmarks. We mark the mouth landmarks as unreliable when CV_{lip} exceeds a calibrated threshold; the underlying intuition is that on assets with a poorly modeled or absent mouth, the landmark detector still emits points, but those points become irregularly spaced. Failing the gate sets the landmark mouth evidence to “unavailable” for the subsequent fusion step. For non-human assets, where human-trained mouth-landmark

Table 4 Per-question signal assignment in the riggability checker. “VLM” uses the semantic signal alone; “Seg mask” replaces a VLM yes/no question with a direct geometric measurement; “Majority” fuses VLM, segmentation, and landmark evidence with a three-way vote.

Q#	Aspect checked	Signal source
Q1	Face type (human / animal / other)	VLM
Q2	Number of visible faces	VLM
Q3	Number of visible eye orbits	VLM
Q4	Mouth present and localizable	Majority
Q5	Eye-region occlusion or obstruction	Seg mask
Q6	Eyewear covering eyes	VLM
Q7	Mouth state	VLM
Q8	Teeth visibility	VLM
Q9	Eye-to-head size ratio	Seg mask
Q10	Lip-seal curvature	Seg mask

Table 5 Geometric criteria evaluated on the face, eye, and mouth segmentation masks. Each criterion produces a binary pass/fail signal that participates in the hybrid decision.

Criterion	Pass condition
Mask presence	face/eye/mouth masks non-empty
Eye inclusion	eye mask inside face boundary
Mouth inclusion	mouth mask inside face boundary
Eye-region occlusion (Q5)	occluder overlap with eye region below threshold
Eye-to-head ratio (Q9)	eye/head area ratio in range
Mouth curvature (Q10)	lip-seal curvature in range

detectors are not reliable, the landmark signal is ignored and the mouth decision is determined by the VLM and the segmentation mask alone.

3.2.4 Mouth-Signal Fusion Logic

The final eligibility decision is the conjunction of all per-question results in Table 4. Q1–Q3 and Q6–Q8 are decided directly by the VLM; Q5, Q9, Q10 are decided by the segmentation-mask checks in Table 5; and Q4 (mouth presence) uses explicit fusion because mouth localization is one of the most common downstream failure sources.

Concretely, for a human-like asset, the mouth decision is:

1. If CV_{lip} exceeds the landmark-quality threshold, treat the landmark evidence as unreliable and rely on the VLM and segmentation signals.
2. Otherwise, take a majority vote over (i) the VLM mouth prediction, (ii) the segmentation-based mouth-detected flag, and (iii) the landmark-based mouth-detected flag.

For non-human assets, the same step degenerates to a conjunction of the VLM and segmentation-mask signals. The majority-vote design recovers the cases that a strict “VLM *and* segmentation” rule would miss when exactly one of the two signals is wrong but the other two agree.

3.2.5 Discussion of Remaining Failure Modes

Empirically, the hybrid VLM+CV checker on the mixed riggability validation set exhibits two dominant failure categories. The first is *annotation borderline cases*, where the ground-truth label itself is ambiguous (e.g., partially occluded faces or stylized characters that are arguably riggable). The second is *VLM-only semantic errors*: misclassification of eyewear, mouth state, or teeth visibility—attributes that segmentation masks and landmarks only partially corroborate. These are the natural targets for future improvement of

the checker, since the geometric and landmark signals have already absorbed most of the failures they are capable of catching.

3.3 Sapiens-Based Segmentation Models

3.3.1 Pretraining

Our learned parser is built on Sapiens-1B (Khironkar et al., 2024), a high-resolution ViT encoder pretrained on a large human-centric web corpus. The pretraining objective follows masked reconstruction: only a subset of patches is visible to the encoder, and the model learns to infer the missing image content from context. For dense human understanding, this inductive bias is particularly useful because the representation remains tied to the observed pixels instead of collapsing purely to global invariances. In practice, it preserves the local appearance and boundary cues that matter for rigging—hairlines, eyelids, lip contours, teeth, and inner-mouth structure—while still learning broad human semantics across pose, clothing, illumination, and style variation. We therefore use the pretrained Sapiens encoder as the common initialization for all Sapiens-based segmentation models in OmniFaceRig. We make two adaptations for our setting: first, we pretrain at 512×512 resolution for efficiency and then briefly switch to 1024×1024 resolution to improve high-resolution facial boundary cues; second, we perform mid-stage unsupervised adaptation on 20M curated in-domain stylized character images. The pretraining corpus contains approximately 4B curated realistic human images. In downstream parsing experiments, these adaptations improve segmentation accuracy by 2–3%, and the in-domain adaptation makes supervised parser training more annotation-efficient.

3.3.2 Segmentation Fine-Tuning

Starting from this pretrained encoder, we attach a lightweight three-stage deconvolutional decoder that upsamples the token grid back to dense logits, and fine-tune only this head while keeping the ViT backbone frozen. We deploy two compatible checkpoints that share the same Sapiens-1B encoder but use different label spaces: a 41-class stylized parser for human-like characters and a 38-class humanoid parser for cartoon animals and strongly non-human characters. The stylized vocabulary retains fine face-specific classes such as facial skin, eyebrows, eyes, ears, lips, teeth, tongue, hair, glasses, and occluders, whereas the humanoid vocabulary trades some granularity for improved stability on cats, dogs, and heavily stylized characters.

To make these parsers practical inside the rigging loop, we package them in a lightweight train-export-infer stack with JSON label configurations and TorchScript checkpoints. This lets the same encoder-decoder family serve dataset curation, ablation, and deployment on standard GPU servers without additional infrastructure. At inference time, OmniFaceRig consumes only the face-relevant channels and collapses them into the geometric cues required downstream: face boundary, eyes, nose or muzzle extent, mouth opening, teeth or inner-mouth support, and accessory-aware occlusion regions.

3.4 Face Detection and Segmentation

Robust face detection and segmentation are critical prerequisites for template fitting.

Render and face detection. For each input asset, we first render the 3D mesh from a frontal viewpoint into a 2D character image, then localize and crop the face region. The cropped face image is the input to all subsequent face-parsing modules.

Multi-model segmentation. Real-time face parsing methods such as BiSeNet (Yu et al., 2018) have achieved strong results on photographic human faces, but AI-generated characters exhibit highly stylized proportions and diverse topologies that challenge any single detector or parser. To maximize coverage, we combine the Sapiens-based parsers from §3.3 with two complementary off-the-shelf models and adaptively select the best result for each facial region:

1. **Face Landmark Detection:** A face detection and landmark model providing 68-keypoint facial landmarks with high precision on human and near-human faces. Used as the primary landmark source for eyes, mouth, and face boundary on human characters.

2. **Sapiens** (Khironkar et al., 2024): The base human parser described in §3.3. It provides strong human nose, lip, and facial-skin estimates, but degrades on strongly non-human faces because of its human-centric training distribution.
3. **SAM 3** (Segment Anything Model 3) (Carion et al., 2025): Building on the Segment Anything foundation (Kirillov et al., 2023) and its video extension SAM 2 (Ravi et al., 2024), SAM 3 is a class-agnostic segmentation foundation model that provides zero-shot segmentation masks from point or box prompts. SAM 3 generalizes well to stylized and non-human faces but produces coarser boundaries compared to landmark-based methods. We use SAM 3 for face region segmentation on characters where face landmark detection and Sapiens fail.
4. **Fine-Tuned Sapiens**: Our stylized and humanoid Sapiens checkpoints from §3.3. The riggability stage selects the 41-class stylized variant for human-like characters and the 38-class humanoid variant for cats, dogs, and heavily stylized assets; these models serve as the primary dense parsers whenever face landmark detection or the base Sapiens model becomes unreliable.

For each input 3D asset, we render the mesh from a frontal viewpoint and run all four models in parallel. The system then *adaptively selects the best detection and segmentation result for each facial part* from the available models. Specifically:

- For *human* assets with standard facial proportions, we rely on face landmark detection (higher precision for eyes and mouth) combined with Sapiens face parsing (for nose and skin regions).
- For *stylized humanoid* assets where face landmark detection may fail due to exaggerated proportions, the system falls back to the 41-class fine-tuned Sapiens parser, which handles non-standard facial proportions more robustly.
- For *animal* assets (felines, canines) where both face landmark detection and standard Sapiens fail, the system uses the 38-class humanoid Sapiens parser (primary) with SAM 3 (fallback) for face boundary and region segmentation.
- Automatic fallback is applied at the per-region level: if the preferred model fails for a specific facial part (e.g., nose segmentation on a cat), the system seamlessly switches to the next-best model for that region only.

The combined multi-model ensemble achieves a face detection recall of nearly 100% across our test sets, compared to 88% for the best single model in isolation. This improvement is especially pronounced on challenging cases: animal characters with fur-covered face boundaries, humanoid characters with exaggerated feature proportions, and characters wearing partial face accessories.

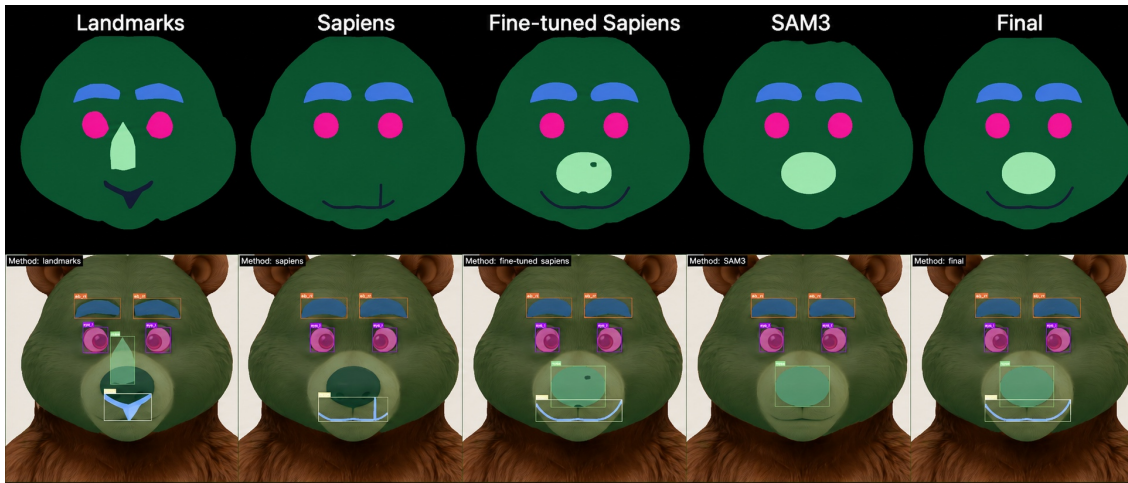
Landmark Extraction (2D & 3D). After segmentation, we extract 2D and 3D keypoints from the final segmentation masks. 2D landmarks for the face boundary, eyes, nose or muzzle, and mouth are read from mask contours and face landmark predictions. We then back-project each 2D landmark onto the input 3D mesh by ray-casting from the rendered camera through the pixel and intersecting the asset surface, yielding the paired 3D position. The resulting 2D + 3D keypoint correspondences are the input to template registration (§3.5).

3.5 Template Registration

3.5.1 Template Design

The core of OmniFaceRig’s face fitting stage is a small library of quad-mesh templates with anchor keypoints, designed for robust fitting across diverse character topologies. The anchor keypoints correspond to facial landmarks (eyes, mouth, face boundary) whose 3D positions are computed from the segmentation ensemble output (§3.4). To accommodate the wide variation in facial shape across topologies, we provide three face template variants, and the VLM (§3.2) automatically selects the appropriate one for each input asset:

- **Human template** — targets human and humanoid characters with conventional facial proportions (flat-fronted face, defined chin, eyes and mouth on roughly the same plane).



(a) Single-model-dominant case.



(b) Ensemble case (per-region fusion needed).

Figure 3 Multi-model face detection and segmentation ensemble. Four models run in parallel; the system adaptively selects the best result per facial region. (a) On a bear, fine-tuned Sapiens already produces a reliable parse and the final result mostly inherits from it. (b) On a fox, fine-tuned Sapiens fails (e.g., spuriously detecting two mouths) and no other single model is fully reliable either; the final mask is assembled by picking the best per-region output across the four models.

- **Long-muzzle template** — targets long-muzzled animals with elongated, forward-protruding snouts, such as dogs, wolves, foxes, and horses.
- **Short-muzzle template** — targets short-muzzled animals with compact or nearly absent snouts, such as cats, bears, rabbits, and tigers.

All three templates share three common design principles that make fitting robust across diverse character types:

- **Nose-landmark-free design.** Anchor target positions are computed by uniformly sampling along the corresponding segmentation-mask boundary, and nose anchors are particularly fragile under this scheme

for two compounding reasons. First, nose segmentation accuracy itself is consistently low on animal faces (feline noses are small and short; canine noses merge into the muzzle) and on many stylized humanoids, so the underlying mask is unreliable. Second, even when the nose mask is plausible, the nose contour tends to be small, irregular, or weakly defined, so uniform boundary sampling yields unstable keypoints that do not correspond across assets. We therefore exclude the nose region from the anchor keypoints entirely; the nose vertices are positioned by the optimization itself, guided by the surrounding border, eye, and mouth anchors. This makes fitting independent of nose segmentation quality, and the resulting nose region naturally adapts to actual face proportions—compact for cats, elongated for dogs, standard for humans.

- **Decoupled fitting and animated topology.** The fitting template (optimized for keypoint correspondence) and the animated topology (designed with radial edge loops around eyes and mouth for muscle-direction deformation) are maintained as separate meshes linked by UV correspondence. This decoupling allows independent optimization: the fitting template can be modified for better landmark matching without affecting the animation-quality edge flow, and vice versa.
- **Minimum region fitting.** The template adheres to the convex hull of facial features rather than extending to the neck and chin. This “minimum region” design produces tighter fits, reduces artifacts at the face-asset merge boundary, and improves robustness on characters with unusual neck or chin geometry (e.g., characters with armor, scarves, or elongated chins).

3.5.2 Keypoint Computation and Fallback Mechanisms

The template fitting relies on dense facial keypoint correspondences between the 68 template anchor vertices and their target positions on the input asset face. These target positions are computed from the segmentation ensemble: eye corners and contours from face landmark detection or fine-tuned Sapiens, mouth corners from landmark detection, and face boundary from segmentation mask edges.

To achieve zero invalid keypoint errors across all test assets, we implement three fallback mechanisms:

1. **Mesh-surface fallback for border keypoints.** After correcting invalid border keypoints to the nearest face mask boundary, some corrected positions still fail 3D projection because the face mask and the actual mesh surface do not perfectly overlap. When a border keypoint has no valid 3D position after mask-boundary correction, we search for the nearest pixel on the actual mesh surface and compute the 3D position directly from the mesh geometry at that pixel.
2. **3D anchor-based fallback.** When a keypoint’s 2D-to-3D projection fails (e.g., the 2D position lands in an area with no mesh geometry), we fall back to computing its 3D position from the already-resolved 3D positions of neighboring anchor keypoints, maintaining a running map of resolved positions so that later keypoints can reference those resolved earlier.
3. **Adaptive eye mask selection.** Both segmentation-based and landmark-based eye masks can contribute to the face boundary computation, but including both can produce an overly large convex hull. We use only one eye mask source, selected adaptively: human assets use landmark-based eyes (higher precision), non-human assets use segmentation-based eyes (more robust), with auto-fallback if the preferred source is unavailable.

3.5.3 Template Fitting Optimization

Given the template mesh and computed keypoint correspondences, the fitting stage deforms the template to match the input asset via a two-stage optimization.

Stage 1: Global Rigid Alignment. We find the best rigid transformation (rotation \mathbf{R} , scale s , translation \mathbf{t}) aligning template keypoints \mathbf{v}_i to asset keypoints \mathbf{p}_i by minimizing:

$$E_{\text{rigid}} = \sum_{i \in \mathcal{K}} \|s\mathbf{R}\mathbf{v}_i + \mathbf{t} - \mathbf{p}_i\|^2 \quad (1)$$

where \mathcal{K} is the set of corresponding keypoints.

Stage 2: Per-Vertex Non-Rigid Deformation. We optimize per-vertex displacements \mathbf{d}_i for all vertices to minimize a composite energy function:

$$E(\mathbf{D}) = \lambda_1 E_{\text{corr}} + \lambda_2 E_{\text{smooth}} + \lambda_3 E_{\text{edge}} + \lambda_4 E_{\text{tri}} + \lambda_5 E_{\text{flip}} + \lambda_6 E_{\text{reg}} \quad (2)$$

where each energy term controls a different aspect of data fitting or geometric regularization to make this fitting pipeline robust to various input cases. The terms are defined as follows:

Correspondence energy (E_{corr}) is the main data term that pulls the template keypoints toward their corresponding asset keypoints:

$$E_{\text{corr}} = \sum_{i \in \mathcal{K}} \mathcal{H}(\|\mathbf{v}'_i - \mathbf{p}_i\|) \quad (3)$$

where $\mathbf{v}'_i = \mathbf{v}_i + \mathbf{d}_i$ represents the deformed template vertex positions, \mathbf{p}_i represents target landmark points, and \mathcal{H} is a robust penalty function such as a Huber loss to ignore outliers.

Smoothness energy (E_{smooth}) enforces smooth deformations by encouraging neighboring vertices connected by a mesh edge \mathcal{E} to move in a similar way:

$$E_{\text{smooth}} = \sum_{(i,j) \in \mathcal{E}} \|\mathbf{d}_i - \mathbf{d}_j\|^2 \quad (4)$$

Edge-length preservation energy (E_{edge}) encourages the deformation to remain locally rigid by preserving original edge lengths up to global scale:

$$E_{\text{edge}} = \sum_{(i,j) \in \mathcal{E}} (\|\mathbf{v}'_i - \mathbf{v}'_j\| - \|\mathbf{v}_i - \mathbf{v}_j\|)^2 \quad (5)$$

Triangle shape preservation energy (E_{tri}) preserves local triangle shapes more strongly than edge-length preservation alone and prevents skinny or sheared triangles:

$$E_{\text{tri}} = \sum_{t \in \mathcal{T}} \|\mathbf{G}_t - \mathbf{G}'_t\|_F^2 \quad (6)$$

where \mathbf{G}_t and \mathbf{G}'_t denote triangle shape matrices encoding the edge lengths and angles before and after deformation, respectively.

Triangle flip penalty (E_{flip}) penalizes orientation reversal and reduces triangle flips and foldovers to prevent self-intersections:

$$E_{\text{flip}} = \sum_{t \in \mathcal{T}} \max(0, -\mathbf{n}_t \cdot \mathbf{n}'_t)^3 \quad (7)$$

where \mathbf{n}_t and \mathbf{n}'_t denote triangle normals before and after deformation, respectively.

Offset regularization energy (E_{reg}) discourages unnecessarily large deformations and improves numerical stability:

$$E_{\text{reg}} = \sum_i \|\mathbf{d}_i\|^2 \quad (8)$$

For normalized meshes, this optimization achieves near-zero alignment error ($< 10^{-5}$). The nose-landmark-free template design and triangle flip penalty ensure zero crashes across all animal assets in Omni-Bench, naturally adapting to diverse face proportions (compact for cats, elongated for dogs) without category-specific tuning.

3.6 Blendshape Rig Construction

Given the fitted face mesh produced by Stage 1 (§3.5), Stage 2 constructs a production-ready FACS blendshape rig in four steps. The original asset is assumed to provide only the visible surface and source textures, with no pre-existing teeth, gums, tongue, or oral-cavity geometry. Stage 2 therefore consumes three additional inputs: the original static asset mesh (for surrounding geometry and source textures), the inner-mouth template selected by the VLM in Stage 1 (§3.2), and a canonical FACS blendshape template.

3.6.1 Face Mesh Fusion

The fitted template positions are first transferred to a high-quality animated topology mesh via UV correspondence, then reprojected onto the input character geometry. Eye regions are inset using virtual eyeball centers (computed via Procrustes alignment of eyelid vertices) to allow eyelid closure without self-intersection. The prepared template then replaces the face region on the original mesh: a 3D convex hull is computed for a subtractive boolean (cut out the old face), the template border vertices are stitched to the remaining mesh boundary via closest-point welding, and small-edge collapse removes degenerate polygons (merge in the new face). This ensures proper radial topology flow around eyes and mouth for high-quality facial deformation. This operation is intentionally local: it preserves the asset’s identity, hairstyle, and non-face geometry while introducing the radial edge flow that downstream expression deformation relies on.

3.6.2 Inner-Mouth Construction

Because the input contains no oral cavity, the inner-mouth geometry (teeth, gums, and tongue) must be synthesized rather than registered. OmniFaceRig synthesizes the missing inner-mouth structures from a small library of inner-mouth template archetypes, summarized in Table 6; the appropriate archetype is selected by the VLM during Stage 1 from the rendered view of the character.

Table 6 Inner-mouth template archetypes and their typical targets. The VLM in Stage 1 selects one archetype per asset, which determines the teeth/gum/tongue template that is warped into the fitted mouth cavity.

Archetype	Typical target characters
Human	realistic humans and humanoid characters
Canine	long-muzzled animals (e.g., dogs, wolves, foxes)
Monster	stylized fantasy creatures with non-standard teeth
Flat	characters with minimal or absent oral structure

The selected teeth template is warped to the fitted mouth interior using Radial Basis Function (RBF) deformation, followed by a rigid transform with non-uniform scale. To prevent teeth protrusion—especially critical for muzzled animal faces—we employ As-Rigid-As-Possible (ARAP) deformation (Sorkine and Alexa, 2007) for initial placement, then iteratively refine using a Signed Distance Field (SDF): the convex hull of the teeth geometry is converted to an SDF, and any face mesh points intersecting the teeth volume are smoothly pushed outward along the SDF gradient. Gum and tongue geometry are fitted simultaneously, connected to the inner mouth surface. This two-stage approach (ARAP + SDF) reliably prevents teeth-face intersections both at rest and during expression activation.

3.6.3 Texture and UV Transfer

After the new face and inner-mouth surfaces are inserted, the global UV layout is rebuilt. UV islands are re-packed using an automated UV layout solver to maximize packing area with no overlap between shells, with sufficient padding to prevent visible seams during MipMap rendering. The face region is scaled up to allocate approximately 10× more texel density than non-face regions, ensuring high-quality facial texture at all LOD levels, and the inner-mouth surfaces are placed on a separate texture channel to keep their material parameters independent. The original texture is resampled onto the new UV layout using a vectorized approach: for each pixel in the output texture, we find the barycentric coordinate and primitive ID on the merged mesh’s UV layout, convert to world-space position, find the closest point on the original mesh, and sample the source texture at the corresponding UV. This preserves the character’s identity and material details while letting the newly synthesized geometry inherit a coherent appearance.

3.6.4 FACS Blendshape Transfer and Post-Processing

Facial expressions are created by transferring blendshapes from the canonical FACS blendshape template to the merged character mesh using sparse deformation transfer (Sumner and Popović, 2004). For each reference shape, triangle-level affine deformations are computed and transferred to the target mesh’s triangle structure, preserving character-specific geometry while reproducing the expression. The transferred shapes are applied

to the merged mesh using Point Deform with Delta Mush smoothing to blend into adjacent non-template regions. Adapting the deformation gradients to the target character’s own proportions is what keeps the transferred expressions character-specific rather than collapsing the rig toward an “average human face,” and is what allows the same set of FACS shapes to be applied to humans, humanoids, long-muzzled animals, and short-muzzled animals without per-character authoring.

Sparse deformation transfer alone cannot enforce certain physical and geometric constraints—eyelids must close without self-intersection, eye-gaze shapes require a known rotation center, jaw motion must move the lower teeth, and extreme mouth poses can re-introduce teeth-face intersections. A small set of expression-specific post-processing rules, summarized in Table 7, handles these cases.

Table 7 Expression-specific post-processing rules applied after sparse deformation transfer. Each rule addresses a constraint that pure deformation transfer cannot enforce on its own.

Shape category	Refinement applied
Closed-eye shapes	upper-eyelid vertices snapped to lower lid and locally relaxed for contact-aware closure
Eye-gaze shapes	eye-region vertices rotate around virtual eyeball centers from Procrustes fit
Jaw-related shapes	lower-teeth subset moves coherently with the jaw, tracking open/close motion
Collision-aware refinement	SDF-based teeth-face penetration check re-applied per expression shape

The system supports three configurable shape-set tiers selected per application: Core (13 shapes) for basic dialog and emotion on mobile characters, Additional (46 shapes) for finer muscle control suitable for mid-fidelity game characters, and Full (155 shapes) for production VR applications where expression fidelity is paramount. The output of Stage 2 is the final FACS blendshape rig, ready to be driven by arbitrary expression weights at run-time.

4 Experiments

Figure 5 presents representative qualitative results across the main topology families in Omni-Bench. Additional qualitative grids extending Figure 5, with more identities, styles, expression frames, and mouth-detail close-ups, are provided in Appendix A.

4.1 Setup

We evaluate OmniFaceRig on the full Omni-Bench dataset (Section 2). All inference-time rigging and evaluation experiments use a single NVIDIA A100 GPU; segmentation model fine-tuning is an offline training step and uses the separate multi-GPU setup described below.

4.2 Implementation Details

Sapiens Pre-Training. We use Sapiens-1B (Khrodkar et al., 2024) as the base segmentation backbone for all Sapiens-based parsers in OmniFaceRig. Following §3.3, the encoder is initialized with masked-reconstruction pretraining: we first train at 512×512 resolution for efficiency, then briefly switch to 1024×1024 resolution for high-resolution facial boundary cues. The pretraining corpus contains approximately 4B curated realistic human images. We then perform a mid-stage unsupervised adaptation on 20M in-domain stylized character images. In our downstream parsing experiments, these two stages improve segmentation accuracy by 2–3%, and the in-domain adaptation makes the subsequent supervised parser training more annotation-efficient.

Fine-Tuned Sapiens Training. To extend Sapiens’ face parsing capability to stylized and non-human characters, we construct a custom training dataset of approximately 10,000 annotated 2D images covering humans, humanoids, and animal species such as felines, canines, ursines, and other stylized creatures, all rendered in

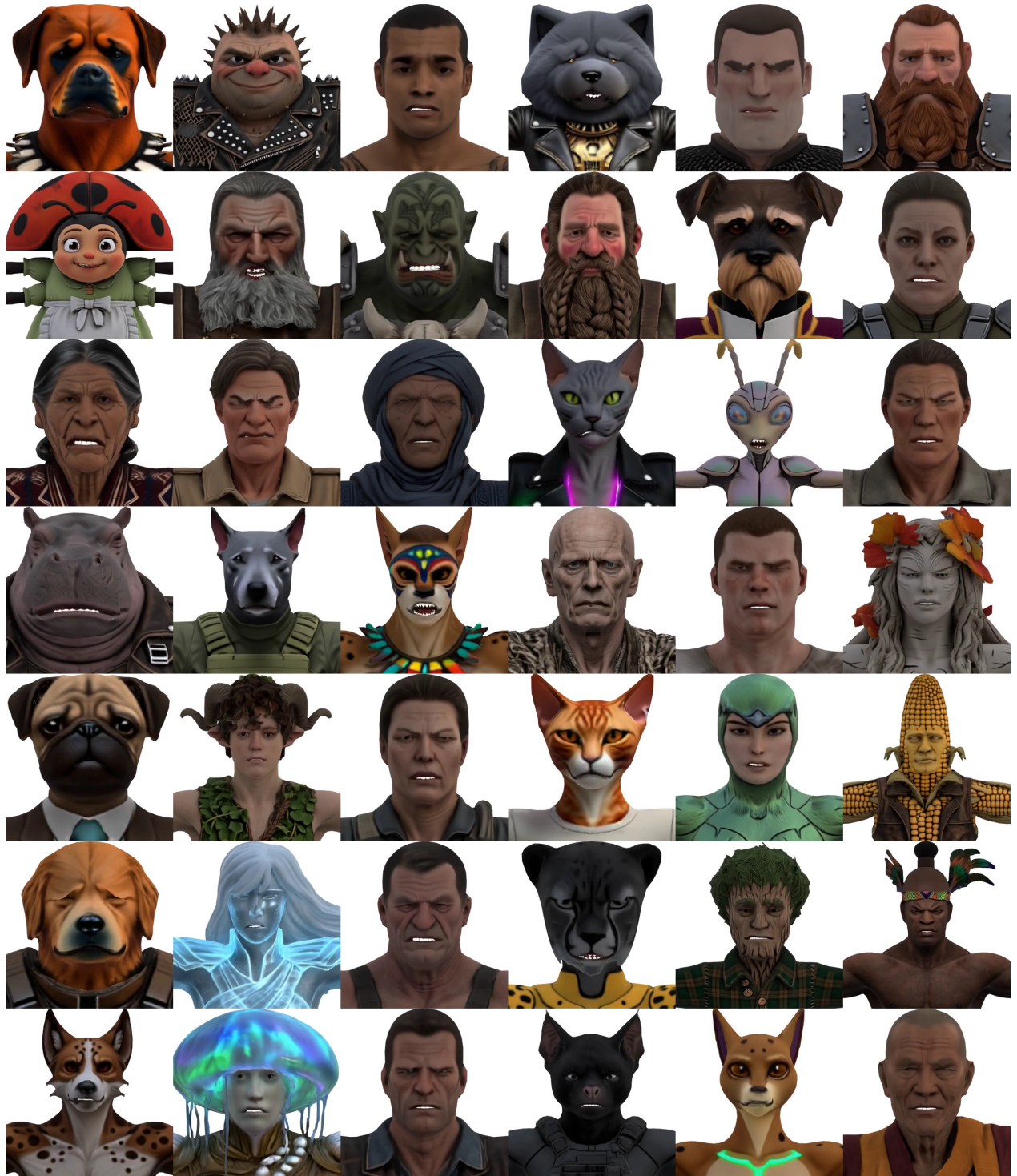


Figure 4 Omni-Bench dataset overview. A sample grid of representative characters from Omni-Bench, spanning humans, humanoids, cats, dogs, and other animals. Each cell shows a rendered frame of the *rigged* asset produced by OmniFaceRig, with the expression sampled at random from the FACS rig (not the static input mesh). Omni-Bench contains 1,000 rigged biped 3D characters in T-pose—500 human and humanoid characters covering 13 occupation archetypes plus stylized fantasy / sci-fi / cyberpunk humanoids, and 500 animals dominated by 150 cats and 150 dogs (10 breeds each) together with 200 other rigging-amenable species (bears, tigers, lions, foxes, wolves, rabbits, etc.). Every asset ships with its full text-to-3D provenance (text prompt, 2D reference image, final mesh) and an auto-generated FACS facial rig of up to 155 blendshapes with procedurally fitted teeth, gums, and tongue.

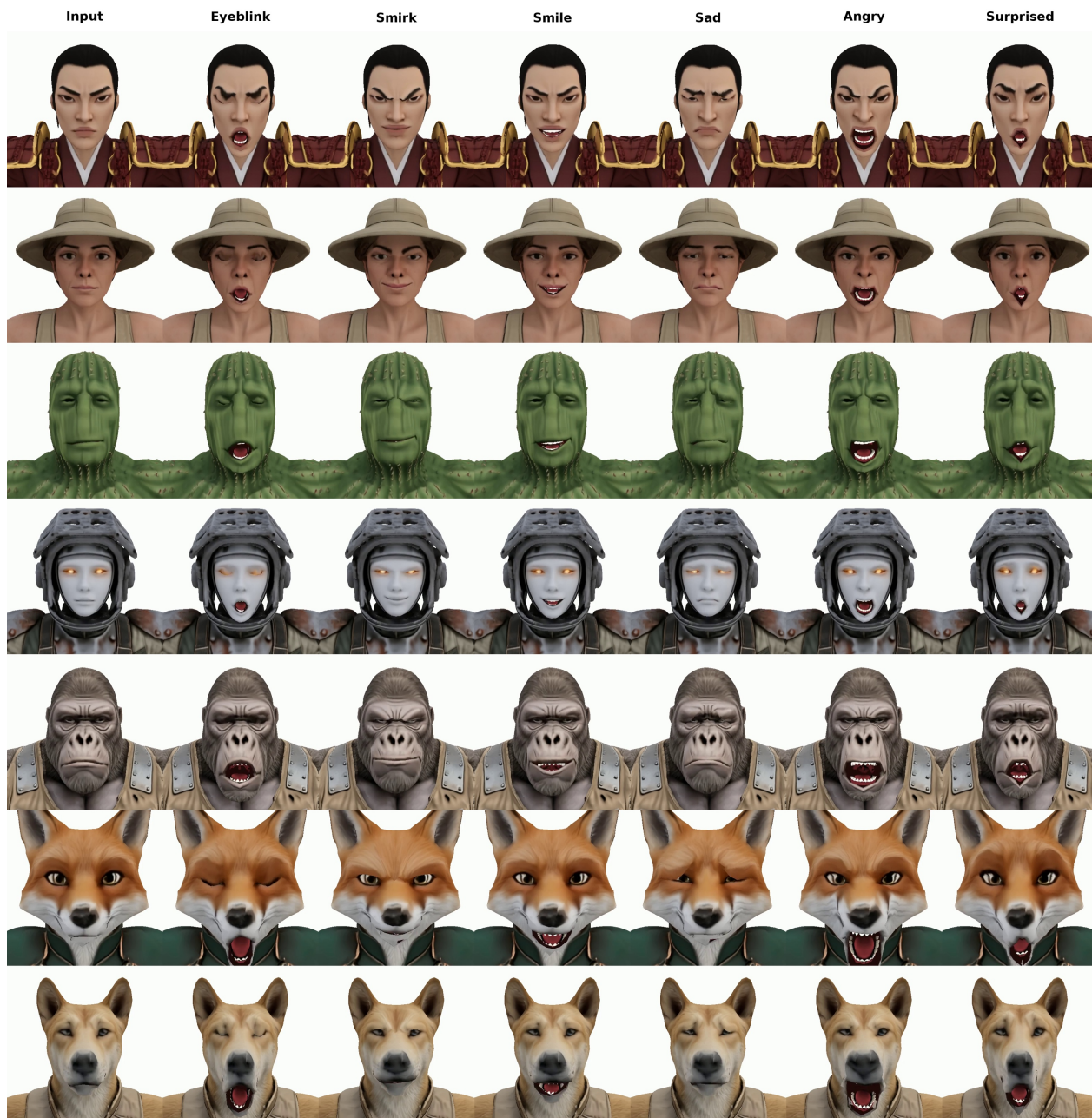


Figure 5 Qualitative OmniFaceRig results across diverse 3D characters from Omni-Bench. Each row is one character. The leftmost column is the input *static surface-only mesh with no pre-modeled oral cavity*; the remaining six columns are generated expression frames labeled at the top (e.g., *surprise, smile, love, anger*), most involving open-mouth deformations that expose the *procedurally generated inner-mouth geometry* (teeth, gums, tongue) synthesized by Stage 2 (§3.6). Rows span the four topology families targeted by OmniFaceRig—realistic and stylized humans, humanoid characters, long-muzzled animals (dogs, wolves, foxes), and short-muzzled animals (cats, bears, tigers)—all produced by the *same* fully automatic pipeline. Three properties are visible across the grid: cross-topology generalization via the three-template + nose-landmark-free design of §3.5; intersection-free inner-mouth geometry under strong expressions via the ARAP+SDF placement of §3.6.2; and preserved character-specific identity from per-character sparse deformation transfer. Additional grids appear in Appendix A.

Table 8 Quantitative comparison with recent facial rigging methods on 200 human/humanoid heads. Baseline numbers (DT, NFR, RigAnyFace) are taken from RigAnyFace (Ma et al., 2025). All meshes are normalized to a unit sphere (radius 1 m). *Requires manual correspondence annotations.

Method	MAE↓ (mm)	Q95↓ (mm)	Penet.↓ (%)
DT (Sumner and Popović, 2004)*	2.93	8.41	–
NFR (Qin et al., 2023)	2.77	7.21	–
RigAnyFace (Ma et al., 2025)	1.01	2.94	0.17
OmniFaceRig (Ours)	0.85	2.50	0.05

frontal T-pose. Starting from the pretrained encoder, we attach a lightweight three-stage deconvolutional decoder and train two compatible parser heads: a 41-class stylized parser for human-like characters and a 38-class humanoid parser for cartoon animals and strongly non-human characters. For evaluation and geometric fitting, these fine-grained labels are collapsed into the face-relevant cues consumed by the rigging pipeline: face boundary, eyes, nose or muzzle extent, mouth opening, teeth or inner-mouth support, and accessory-aware occlusion regions.

During fine-tuning, we freeze the Sapiens-1B ViT encoder to preserve its open-world visual features and train only the segmentation decoder heads. Training uses AdamW with a learning rate of 1×10^{-4} , cosine decay with 500 warmup steps, batch size 16, and class-balanced cross-entropy loss for imbalanced facial regions. Training runs for 50 epochs on $8 \times$ NVIDIA A100 GPUs, taking approximately 24 hours. We apply standard data augmentation: random horizontal flip, color jitter, random rotation ($\pm 15^\circ$), and random scale ($0.8\text{--}1.2\times$).

The fine-tuned parsers achieve a mean Intersection-over-Union (mIoU) of 87.3% on our held-out test set after collapsing predictions to the rigging-relevant facial cues, compared to 62.1% for the original Sapiens parser. The improvement is most pronounced on animal faces: cat face mIoU improves from 31.2% to 84.5%, and dog face mIoU from 28.7% to 81.9%, while human face mIoU remains stable ($89.1\% \rightarrow 91.2\%$).

4.3 Evaluation Metrics and Baselines

Drawing upon the evaluation protocols used by recent facial rigging methods (Ma et al., 2025; Qin et al., 2023; Cha et al., 2025), we employ a comprehensive set of metrics. We use Mean Absolute Error (MAE) and 95th-Percentile Vertex Error (MAE Q95) to measure the mean and worst-case per-vertex Euclidean distance between the predicted expression mesh and ground truth (normalized to a unit sphere). Penetration Rate measures the percentage of penetrating vertices between inner-mouth components (teeth, gums, and tongue) and the outer facial surface. To quantify pipeline robustness, we introduce Success Rate, tracking the percentage of successfully rigged assets among screened candidate inputs that have passed the VLM+CV riggability checker. Finally, Processing Latency measures the end-to-end execution time in seconds.

For in-the-wild and non-humanoid evaluation, we utilize our proposed Omni-Bench.

We benchmark our method against the most relevant recent baselines: Neural Face Rigging (NFR) (Qin et al., 2023), a pioneering neural method for in-the-wild facial meshes; Deformation Transfer (DT) (Sumner and Popović, 2004), the classic geometric baseline; and RigAnyFace (Ma et al., 2025), a strong recent method supporting disconnected components.

4.4 Quantitative Results

Table 8 presents the quantitative comparison against recent methods on 200 human/humanoid heads. OmniFaceRig achieves the lowest mean vertex error (MAE: 0.85 mm) and worst-case error (MAE Q95: 2.50 mm), outperforming RigAnyFace by 16% and 15% respectively. Our collision-aware deformation transfer reduces the penetration rate to 0.05%, a $3.4\times$ improvement over RigAnyFace, ensuring clean separation between inner-mouth components (teeth, gums, and tongue) and the outer facial surface. Beyond alignment quality, OmniFaceRig also runs the full pipeline reliably on this screened evaluation set, with the riggability

Table 9 Quantitative comparison on a 300-asset human + humanoid subset of Omni-Bench. We restrict this evaluation to humans and stylized humanoids because DT and NFR are designed for human facial topology and do not generalize to non-human characters. RigAnyFace (Ma et al., 2025) is not included here because its code is not publicly available, so it cannot be re-evaluated on Omni-Bench. *Requires manual correspondence annotations.

Method	MAE↓ (mm)	Q95↓ (mm)	Penet.↓ (%)	Succ.↑ (%)
DT (Sumner and Popović, 2004)*	3.12	9.05	–	82.4
NFR (Qin et al., 2023)	2.95	8.11	–	85.1
OmniFaceRig (Ours)	0.92	2.71	0.08	99.0

Table 10 Ablation: segmentation model contribution. Face detection recall (%) on Omni-Bench. The four-model ensemble achieves nearly perfect recall by combining each model’s strengths.

Model Config	Human	Cat	Dog	Overall
Face landmark only	92%	12%	18%	41%
Sapiens only	88%	35%	42%	55%
SAM 3 only	78%	71%	68%	72%
Fine-tuned Sapiens only	90%	89%	85%	88%
4-model ensemble (Ours)	100%	100%	97%	~99%

checker filtering out unsupported inputs and the remaining assets all producing complete rigs. Note that OmniFaceRig evaluates a broader pipeline than the compared baselines (face fusion, inner-mouth synthesis, UV/texture re-bake, and FACS transfer in addition to surface alignment), and its 20–30 s end-to-end runtime on a single A100 GPU includes data I/O, which itself accounts for roughly 10–15 s of the total; the per-stage breakdown is reported in §4.6.

Table 9 presents the evaluation on a 300-asset subset of Omni-Bench that combines realistic humans and stylized humanoids. We restrict this comparison to humans and humanoids because DT and NFR are designed for human facial topology and do not produce meaningful results on non-human characters; including them on Omni-Bench animal assets would not be a fair comparison. The evaluated inputs have first passed the initial VLM+CV riggability screen, which filters out assets with missing faces, severe occlusions, non-standard orientations, or unsupported facial topologies. On this human + humanoid subset, traditional methods like DT and early learning-based methods like NFR struggle with the stylized humanoid characters, while OmniFaceRig maintains sub-millimeter alignment error, a low penetration rate, and a near-perfect 99.0% final rigging success rate. Across the broader Omni-Bench set including animals, OmniFaceRig further exhibits zero crashes on all animal assets thanks to our multi-stage keypoint fallback mechanisms. Figure 5 shows qualitative rigging results across diverse character types and expression frames; additional qualitative grids covering more identities, styles, and topology families are provided in Appendix A.

4.5 Ablation Studies

Segmentation Model Ablation. We evaluate the contribution of each model in our four-model ensemble by measuring face detection recall on Omni-Bench when using each model individually versus the full ensemble (Table 10).

Face landmark detection provides high precision on human faces (92%) but fails almost entirely on animals (12–18%), as it is trained exclusively on human face data. Standard Sapiens degrades on non-human faces (35–42%) due to its human-centric training, despite being a strong foundation model. SAM 3 offers the broadest single-model coverage (72% overall) due to its class-agnostic design, but provides coarser segmentation boundaries than landmark-based methods. Fine-tuned Sapiens substantially improves animal face detection (85–89%) while retaining strong human performance (90%), validating the effectiveness of our fine-tuning strategy. The four-model ensemble with adaptive per-region selection achieves nearly 100% overall recall by combining the precision of face landmark detection on humans, fine-tuned Sapiens’ robustness on animals, and SAM 3’s fallback coverage for edge cases.



Figure 6 Why nose anchors are unreliable. Across five representative assets the nose region exhibits dramatic variation in both detection quality and contour shape. From left to right: (1) a human with a clean, well-detected nose (a positive baseline); (2) a human where nose detection outright fails; (3) a stylized humanoid where detection returns a mask but the contour is oddly shaped; (4) an animal where detection succeeds but the mask has the wrong overall nose shape; and (5) an animal where detection technically succeeds but the nose mask merges with the mouth into an irregular contour. Rows (top to bottom): input asset render; final nose segmentation mask; asset render with the mask overlaid. Even when detection succeeds, the strongly varying nose contour means that uniformly-sampled boundary keypoints do not correspond across assets, motivating our nose-landmark-free template design (§3.5).

Nose Landmark Ablation. We evaluate the impact of our nose-landmark-free template design on animal face rigging quality. When nose anchor keypoints are included (as in prior template designs), the pipeline produces severely distorted nose-mouth regions on 78% of animal assets and crashes on 10%, driven by the two failure modes discussed in §3.5: incorrect nose segmentation, and—even when the nose mask is plausible—unstable keypoints from uniform boundary sampling on small, irregular nose contours. Removing nose anchors and allowing the optimization to position the nose region from the surrounding border, eye, and mouth anchors eliminates these distortion artifacts and reduces the crash rate to 0% across all animal assets in Omni-Bench. Figure 6 provides visual evidence for both failure modes across a range of character topologies.

Riggability Checker. The hybrid VLM+CV approach outperforms either component alone (Table 3): the VLM provides strong archetype identification and accessory detection, while CV filtering catches geometric edge cases (no-face assets, degenerate meshes).

4.6 Latency Breakdown

The face pipeline executes on a single NVIDIA A100 GPU. End-to-end latency is approximately 20–30s per asset, including data I/O. Stage 1 (riggability assessment, face parsing, keypoint extraction, and template fitting) takes 8–10s, while Stage 2 (mesh fusion, inner-mouth fitting, UV/texture processing, and blendshape transfer) takes 10–15s. Compared to manual sculpting workflows that typically take hours to days, this represents a reduction of 2–3 orders of magnitude.

5 Related Work

5.1 3D Asset and Character Generation

Text-to-3D and image-to-3D generation have rapidly lowered the barrier to creating 3D assets. Score-distillation methods such as DreamFusion (Poole et al., 2023) and Magic3D (Lin et al., 2023) optimize a NeRF or mesh through a 2D diffusion prior, while feed-forward latent-diffusion approaches such as Shap-E (Jun and Nichol, 2023), reference-conditioned models such as Zero-1-to-3 (Liu et al., 2023), and fast textured reconstruction systems such as SF3D (Boss et al., 2024) produce 3D objects directly from a text prompt or a single reference image. Meta 3D AssetGen (Siddiqui et al., 2024) targets higher-quality text-to-mesh generation with geometry, texture, and PBR materials, while AssetGen2 (Ranjan et al., 2025) extends this line of asset-generation models and has been used as the image-to-3D base model in WorldGen (Wang et al., 2025b), a representative text-to-3D world-generation system. Character-focused systems narrow this generic capability in two ways: Make-it-vivid (Tang et al., 2024) stylizes and re-textures existing 3D characters, and Make-a-character (Ren et al., 2023) composes textured anime-style avatars from descriptive text. A parallel wave of commercial 3D-generation services has made static character asset creation accessible to non-expert users at production scale. However, most of these systems focus on the visible exterior surface: their outputs are static textured meshes, but they typically do not include animation-oriented facial topology (such as radial edge loops around eyes and mouth), FACS blendshape controls, or complete oral-cavity geometry (teeth, gums, tongue) needed for inner-mouth-aware animation. OmniFaceRig is therefore complementary to this line of work: it takes surface-only meshes of the kind produced by modern 3D generators and lifts them into animation-ready facial rigs in a fully automatic step, without sending the asset back to the generator or requiring manual cleanup of the produced geometry.

5.2 Parametric Face Models vs. Blendshape Rigging

Parametric face models provide statistical representations of human facial geometry. The 3D Morphable Model (3DMM) (Blanz and Vetter, 1999), FaceWarehouse (Cao et al., 2014), and FLAME (Li et al., 2017) established compact linear shape spaces for face reconstruction by capturing the principal modes of identity and expression variation in scanned human faces. Multilinear extensions (Brunton et al., 2014; Vlastic et al., 2006) explicitly factor identity from expression, and disentangled latent representations (Abrevaya et al., 2019; Jiang et al., 2019) further isolate semantic shape components for more flexible control. Image-driven reconstruction methods such as CoMA (Ranjan et al., 2018)—a graph-convolutional autoencoder defined on a fixed mesh topology—and DECA (Feng et al., 2021)—which regresses FLAME coefficients plus per-vertex detail displacements from a single in-the-wild image—leverage these models to recover animatable faces directly from photographs or video. By design, however, these models are usually bound to a fixed mesh topology and expression basis defined at scan-collection time, and they primarily assume adult human anatomy: applying them to a novel asset with arbitrary topology, stylized proportions, or non-human features often requires re-fitting a new mesh into the parametric basis (which can lose character-specific identity) or leads to unstable fits. OmniFaceRig sidesteps this constraint: it does not project the input asset into a fixed parametric space but instead deforms small topology-specific templates to match the input geometry, producing a character-specific blendshape set defined on the asset’s own surface.

In contrast to the parametric line, production pipelines rely on the Facial Action Coding System (FACS) (Ekman and Friesen, 1978) and per-character blendshape rigs (Lewis et al., 2014; Lewis and Anjyo, 2010), which give animators intuitive, localized control while preserving character-specific geometry (Seol et al., 2011; Kavan et al., 2024). Orvalho et al. (Orvalho et al., 2012) survey the broader rigging landscape, covering the multi-decade evolution from fully manual sculpting toward semi-automatic, template-based pipelines. On the representation side, spectral methods have been explored for compact animation encoding (Wang et al., 2015), but a dominant production cost is still the per-character authoring effort of producing a complete FACS blendshape set, which historically requires a skilled technical artist for each new asset. Our method follows the production blendshape paradigm but removes the per-character authoring step targeted by our pipeline: from a single surface-only input mesh, OmniFaceRig procedurally constructs a full FACS rig and inner-mouth geometry without per-character template tuning or hand sculpting.

5.3 Traditional and Learning-Based Facial Auto-Rigging

Traditional methods. Noh and Neumann (Noh and Neumann, 2001) introduced expression cloning by directly transferring per-vertex displacements between a source and target face mesh. Sumner and Popović (Sumner and Popović, 2004) reformulated this as deformation transfer over triangle-level affine transformations, providing a principled foundation that handles modest topology changes and is the kernel our blendshape transfer stage builds upon. Orvalho et al. (Orvalho et al., 2008) extended deformation transfer to retarget an entire FACS rig across different face models, while Li et al. (Li et al., 2010) demonstrated example-based facial rigging from a small set of artist-authored exemplar shapes. Seol et al. (Seol et al., 2012) added a spacetime formulation to clone temporally coherent expressions across blendshape systems, Liu et al. (Liu et al., 2011) proposed a unified framework for locally retargeting and rendering facial performance, and Ribera et al. (Ribera et al., 2017) addressed retargeting with automatic range-of-motion alignment between rigs whose deformation scales differ. These methods can produce high-quality outputs but share a common bottleneck: they assume carefully established dense correspondences between source and target meshes, often with manual setup. That correspondence step limits scalability to in-the-wild generated 3D assets, where topology and part structure vary widely across characters. OmniFaceRig retains the deformation-transfer kernel of Sumner and Popović but replaces the manual correspondence step with the segmentation-driven, dense keypoint registration of Stage 1, making the pipeline run unattended on arbitrary input meshes.

Learning-based methods. Early data-driven approaches relied on direct regression: Li et al. (Li et al., 2020a) used CNNs over geometry images to predict per-vertex blendshape offsets, and Chandran et al. (Chandran et al., 2022b, 2020) introduced semantic deformation transfer that maps shape changes by semantic correspondence rather than triangle alignment, later refining the formulation with transformer architectures for topology-independent shape transfer (Chandran et al., 2022a). Interactive editing has been explored through sketch-based blendshape interfaces (Cetinaslan and Orvalho, 2020a,b), BSGen (Wang et al., 2023b) demonstrated automatic blendshape generation by learning a generative model over canonical shapes, and Ming et al. (Ming et al., 2024) produced high-quality mesh blendshapes from monocular face videos via neural inverse rendering. On the representation side, MeshCNN (Hanocka et al., 2019) and DiffusionNet (Sharp et al., 2022) provide mesh-native learned features that have been broadly adopted as encoder backbones for downstream rigging tasks.

The recent wave of in-the-wild neural face rigging methods is closest in spirit to OmniFaceRig. Neural Face Rigging (NFR) (Qin et al., 2023) pioneered topology-agnostic neural deformation by learning a per-shape latent code together with a graph-conditioned decoder that generalizes across human face meshes; however, NFR operates on a single connected outer-surface component, does not handle disconnected sub-meshes (eyes, teeth, eyelashes), and is trained on human data. FaBRig (Zhu and Joslin, 2024) proposes a cloth-simulation-inspired transferable 3D face parameterization that improves robustness to topology variation, but still targets human faces. Neural Facial Deformation Transfer (NFDT) (Chandran et al., 2025) replaces the GNN/encoder–decoder design with a decoder-only transformer for high-fidelity transfer, while Neural Face Skinning (NFS) (Cha et al., 2025) proposes mesh-agnostic skinning weights that can in principle handle disconnected components, although NFS produces a skinning rig rather than a FACS blendshape set. RigAnyFace (Ma et al., 2025) is a strong recent system in this family and supports disconnected components at training scale by leveraging 2D supervision over unlabeled in-the-wild face data. However, these learning-based systems generally focus on outer-surface facial deformation: they do not synthesize the interior teeth/gums/tongue geometry needed for inner-mouth-aware expressions, and their training and evaluation are centered on human faces. Most recently, CANRig (Research, 2026) adds cross-attention mechanisms for variable local control of neural face rigs, and ControlFace (Jang et al., 2025) harnesses 3DMM-conditioned rendering for more flexible face rigging—both remain tied to human facial anatomy. Zero-shot stylization approaches (Wang et al., 2023a) and portrait animation methods such as MegActor (Yang et al., 2024) target stylized characters but operate in 2D image space, not as 3D blendshape rigs. DreamFace (Zhang et al., 2023) generates animatable 3D faces under text guidance, but it is a face *generator* that synthesizes characters from prompts, not a *rigger* that takes an existing static asset and adds animation. Relative to these lines of work, OmniFaceRig addresses two gaps that remain important for generated-character production: it procedurally synthesizes inner-mouth geometry (teeth, gums, and tongue) from a surface-only input mesh, and it generalizes the same rigging pipeline to non-human topologies—long- and short-muzzled animals—via topology-specific templates with no retraining (see Table 2 in §3 for a feature-level comparison).

5.4 Neural Face Avatars

A parallel line of work reconstructs animatable head avatars using neural scene representations rather than explicit mesh rigs. Early neural radiance field (NeRF) methods demonstrated photorealistic novel-view synthesis of faces but lacked fine-grained expression control. The advent of 3D Gaussian Splatting (3DGS) shifted the field toward explicit point-based primitives that achieve real-time rendering while retaining differentiable optimization. GaussianAvatars (Qian et al., 2024) pioneered this direction by binding 3D Gaussians to the triangles of a parametric FLAME mesh, enabling full pose and expression control at photorealistic quality. HeadGaS (Dhamo et al., 2024) extended 3DGS to real-time animatable head avatars via a hybrid model that conditions Gaussian attributes on expression codes, while FlashAvatar (Xiang et al., 2024) embedded Gaussians in the UV space of a FLAME mesh for lightweight, high-fidelity reconstruction from short monocular videos.

More recently, 3D Gaussian Blendshapes (Ma et al., 2024) introduced a representation directly analogous to classical mesh blendshapes: a neutral Gaussian model plus per-expression Gaussian offsets that are linearly blended with FACS-like coefficients. RGBAvatar (Li et al., 2025) further streamlines this design by predicting a reduced blendshape basis from FLAME expressions, achieving online avatar reconstruction in under two minutes from a monocular video. MeGA (Wang et al., 2025a) proposes a hybrid mesh–Gaussian approach that models the face with an enhanced FLAME mesh and the hair with deformable 3D Gaussians, enabling high-fidelity rendering and downstream editing such as hairstyle alteration. Gaussian Eigen Models (GEM) (Zielonka et al., 2025) take a network-free approach by representing head avatars as linear combinations of Gaussian eigen-bases, providing lightweight and easily controllable avatars without runtime neural network inference. FATE (Zhang et al., 2025) reconstructs a full 360° head avatar with textural editing capabilities from a single monocular video. Avat3r (Kirschstein et al., 2025), developed concurrently at Meta, builds a large reconstruction model that regresses an animatable 3D Gaussian head avatar from just a few input images in a single forward pass, vastly reducing per-identity optimization.

Despite their impressive rendering quality, these neural-avatar methods are primarily *rendering-focused*: they produce neural scene representations optimized for novel-view image synthesis rather than editable mesh assets. Their outputs are generally not directly exportable as standard blendshape rigs compatible with game engines, offline renderers, or production facial motion-capture retargeting pipelines. They are also trained around human head data and do not directly target animal or stylized non-human characters. Finally, inner-mouth structures such as teeth, gums, and tongue are typically represented only through appearance, if at all, rather than as explicit editable geometry. OmniFaceRig addresses a complementary problem: given an existing static mesh, including one generated by a 3D content creation model, it produces an explicit, topology-preserving FACS blendshape rig with procedurally fitted inner-mouth structures, and generalizes across human, humanoid, and animal topologies without retraining.

5.5 Rigging for Non-Humanoid Characters

Extending facial rigging to non-humanoid characters remains challenging because of the wide anatomical gap between human and animal faces—in muzzle length, eye placement, jaw articulation, fur coverage, and the inner-mouth structure itself (Danieau et al., 2019). The parametric-modeling line of work has produced quadruped *shape* models such as SMAL (Zuffi et al., 2017) and BARC (Rüegg et al., 2023), which capture body and pose variation across animal species using category-specific shape priors fitted from scans and silhouettes. These models are highly effective for animal body reconstruction and pose estimation, but they do not address facial rig construction or blendshape generation: the head is represented as a low-dimensional shape component rather than as an animatable, expression-driven facial rig. On the perception side, Cheng et al. (Cheng et al., 2024) addressed the domain gap between photographic human faces and artistic character designs by training facial landmark detectors that cover stylized characters as well; this kind of perception layer is a useful building block but does not close the rigging loop on its own. The recent in-the-wild neural rigging methods discussed above (Qin et al., 2023; Ma et al., 2025) are trained primarily on human face datasets and inherit human-centric inductive biases (eye placement, nose shape, mouth contour), which limits their direct transfer to cats, dogs, and stylized non-human characters. These lines of work leave two practical gaps for animal rigging: (i) they focus on the outer facial surface and do not construct explicit oral-cavity geometry, even though teeth and tongue layout differ dramatically between humans, canines,

felines, and stylized creatures; and (ii) they rely on a single facial-anatomy prior or trained model, whereas generated animals often require topology-specific handling. OmniFaceRig targets this setting directly: a robust multi-model segmentation ensemble identifies facial regions across species, a small library of topology-specific templates (human, long-muzzle, short-muzzle) handles geometric diversity without retraining, and procedurally fitted inner-mouth archetypes with ARAP+SDF placement produce clean inner-mouth geometry adapted to the species-specific oral structure of the input asset.



Figure 7 Failure cases. From left to right: (1) a *bird* with a sharp beak and an unusual surface around the beak that segmentation cannot localize as a standard face; (2) a *fish-like face* with a very wide, elongated mouth that extends almost to the face boundary, on which segmentation tends to fill in the mouth region incorrectly; (3) an *insect* with oversized compound eyes located near the face boundary and an irregular mouth layout that disrupts landmark detection; (4) a *seahorse-like animal* with a strongly elongated or flattened snout (or a heavily occluded mouth) whose facial topology falls outside our template families. Rows (top to bottom): input render; final segmentation mask; asset render with the mask overlaid. In all four cases, segmentation either breaks down or the underlying face/mouth anatomy cannot be reliably fit by any of our human, long-muzzle, or short-muzzle templates.

6 Conclusions and Limitations

We presented OmniFaceRig, a fully automatic inner-mouth-aware face rigging pipeline for 3D characters. Given a static surface-only 3D mesh with no pre-modeled oral cavity, OmniFaceRig produces a production-ready rig with up to 155 FACS blendshapes and procedurally generated inner-mouth geometry (teeth, gums, and tongue), with no manual intervention at any stage. Our four-model detection and segmentation ensemble, combined with a nose-landmark-free template design, enables robust fitting across diverse 3D character topologies—humans, humanoids, long-muzzled animals, and short-muzzled animals—with sub-millimeter alignment error and zero pipeline crashes across all animal assets in Omni-Bench, while ARAP+SDF teeth placement keeps inner-mouth geometry intersection-free even for muzzled species. Together with the method, we make Omni-Bench publicly available as a benchmark dataset of 1,000 rigged biped characters with FACS

facial blendshapes and inner-mouth geometry, to catalyze future research in automatic facial rigging.

Limitations. While OmniFaceRig significantly advances automatic facial rigging, it still has limitations. The current system is designed for visible-faced characters whose facial topology falls within our human, long-muzzle, and short-muzzle template families. Specialized animals with qualitatively different mouth and face anatomy—for example birds with sharp beaks, fish-like faces with flat snouts, insects with oversized compound eyes, or animals with unusually elongated snouts (Figure 7)—may be rejected by the riggability checker or produce unreliable fits even when segmentation succeeds. More generally, our template-family design improves robustness over a single universal template, but it does not provide a fully general facial parameterization for every possible animal or stylized character; extending coverage to new topology families will require additional templates, segmentation labels, and riggability criteria. Finally, although the 20–30 s runtime is fast relative to manual rigging, the current multi-stage pipeline is still better suited for offline or batch asset processing than real-time interactive editing. Future work will explore broader topology families, more adaptive template generation, and tighter integration of the perception and geometry stages.

References

- Victoria F Abrevaya, Adnane Boukhayma, Stefanie Wuhler, and Edmond Boyer. A decoupled 3d facial shape model by adversarial training. In *International Conference on Computer Vision (ICCV)*, 2019.
- Volker Blanz and Thomas Vetter. A morphable model for the synthesis of 3d faces. In *SIGGRAPH*, pages 187–194, 1999.
- Mark Boss, Zixuan Huang, Aaryaman Vasishtha, and Varun Jampani. SF3D: Stable fast 3D mesh reconstruction with UV-unwrapping and illumination disentanglement. *arXiv preprint arXiv:2408.00653*, 2024.
- Alan Brunton, Timo Bolkart, and Chenglei Wu. Multilinear wavelets: A statistical shape space for human faces. In *European Conference on Computer Vision (ECCV)*, 2014.
- Chen Cao, Yanlin Weng, Shun Zhou, Yiying Tong, and Kun Zhou. Facewarehouse: A 3d facial expression database for visual computing. *IEEE Transactions on Visualization and Computer Graphics*, 20(3):413–425, 2014.
- Nicolas Carion, Laura Gustafson, Yuan-Ting Hu, Shoubhik Debnath, Ronghang Hu, Didac Suris, Chaitanya Ryali, Kalyan Vasudev Alwala, Haitham Khedr, Andrew Huang, et al. SAM 3: Segment anything with concepts. *arXiv preprint arXiv:2511.16719*, 2025.
- Ozan Cetinaslan and Verónica Orvalho. Sketching manipulators for localized blendshape editing. *Graphical Models*, 108:101059, 2020a.
- Ozan Cetinaslan and Verónica Orvalho. Stabilized blendshape editing using localized jacobian transpose descent. *Graphical Models*, 112:101091, 2020b.
- Seyeon Cha, Seongwon Yoon, Kyungjin Seo, and Junhyeok Noh. Neural face skinning for mesh-agnostic facial expression cloning. *Computer Graphics Forum (CGF)*, 44(2):e70009, 2025.
- Prashanth Chandran, Derek Bradley, Markus Gross, and Thabo Beeler. Semantic deep face models. In *International Conference on 3D Vision (3DV)*, 2020.
- Prashanth Chandran, Loïc Ciccone, Markus Gross, and Derek Bradley. Local anatomically-constrained facial performance retargeting. *ACM Transactions on Graphics (TOG)*, 41(4):168:1–168:14, 2022a.
- Prashanth Chandran, Gaspard Zoss, Markus Gross, Paulo F U Gotardo, and Derek Bradley. Shape transformers: Topology-independent 3d shape models using transformers. *Computer Graphics Forum (CGF)*, 41(2):195–207, 2022b.
- Prashanth Chandran, Loïc Ciccone, Gaspard Zoss, and Derek Bradley. Neural facial deformation transfer. In *Eurographics*, 2025.
- Shiyang Cheng et al. Facial landmark detection for stylized characters. In *ACM Multimedia (ACM MM)*, 2024.
- Daniel Cudeiro et al. Capture, learning, and synthesis of 3d speaking styles. In *Computer Vision and Pattern Recognition (CVPR)*, 2019.
- Fabien Danieau, Ivan Gubins, Nicolas Olivier, Olivier Dumas, et al. Automatic generation and stylization of 3d facial rigs. In *IEEE Conference on Virtual Reality and 3D User Interfaces (VR)*, 2019.
- Yufan Deng, Yuhao Zhang, Chen Geng, Shangzhe Wu, and Jiajun Wu. Anymate: A dataset and baselines for learning 3d object rigging. *arXiv preprint arXiv:2505.06227*, 2025.
- Helisa Dharmo, Yinyu Nie, Arthur Moreau, Jifei Song, Richard Shaw, Yiren Zhou, and Eduardo Pernía Delgado. Headgas: Real-time animatable head avatars via 3d gaussian splatting. In *European Conference on Computer Vision (ECCV)*, pages 456–474, 2024.
- Paul Ekman and Wallace V Friesen. *Facial Action Coding System: A Technique for the Measurement of Facial Movement*. Consulting Psychologists Press, Palo Alto, CA, 1978.
- Yao Feng, Haiwen Feng, Michael J Black, and Timo Bolkart. Learning an animatable detailed 3d face model from in-the-wild images. *ACM Transactions on Graphics (TOG)*, 40(4):88:1–88:13, 2021.
- Rana Hanocka, Amir Hertz, Noa Fish, Raja Giryes, Shachar Fleishman, and Daniel Cohen-Or. Meshcnn: a network with an edge. *ACM Transactions on Graphics (TOG)*, 38(4):90:1–90:12, 2019.
- Wonhyeok Jang et al. ControlFace: Harnessing facial parametric control for face rigging. In *Computer Vision and Pattern Recognition (CVPR)*, 2025.

- Zi-Hang Jiang, Qianyi Wu, Keyu Chen, and Juyong Zhang. Disentangled representation learning for 3d face shape. In *Computer Vision and Pattern Recognition (CVPR)*, 2019.
- Heewoo Jun and Alex Nichol. Shap-e: Generating conditional 3d implicit functions. *arXiv preprint arXiv:2305.02463*, 2023.
- Ladislav Kavan, John Doublestein, Martin Prazak, Matthew Cioffi, and Doug Roble. Compressed skinning for facial blendshapes. In *SIGGRAPH*, 2024.
- Rawal Khirodkar, Timur Bagautdinov, Julieta Martinez, Su Zuo, James Austin, Roshan Zheng, et al. Sapiens: Foundation for human vision models. In *European Conference on Computer Vision (ECCV)*, 2024.
- Alexander Kirillov, Eric Mintun, Nikhila Ravi, Hanzi Mao, Chloe Rolland, Laura Gustafson, Tete Xiao, Spencer Whitehead, Alexander C Berg, Wan-Yen Lo, Piotr Dollár, and Ross Girshick. Segment anything. In *International Conference on Computer Vision (ICCV)*, pages 4015–4026, 2023.
- Tobias Kirschstein, Javier Romero, Simon Giebenhain, and Matthias Nießner. Avat3r: Large animatable gaussian reconstruction model for high-fidelity 3d head avatars. In *International Conference on Computer Vision (ICCV)*, 2025.
- J P Lewis and Ken-ichi Anjyo. Direct manipulation blendshapes. *IEEE Computer Graphics and Applications*, 30(4): 42–50, 2010.
- J P Lewis, Ken Anjyo, Taehyun Rhee, Mengjie Zhang, Frederic H Pighin, and Zhigang Deng. Practice and theory of blendshape facial models. In *Eurographics State of the Art Reports (EG STAR)*, 2014.
- Hao Li, Thibaut Weise, and Mark Pauly. Example-based facial rigging. *ACM Transactions on Graphics (TOG)*, 29(4):32:1–32:6, 2010.
- Jiaman Li, Zhengfei Kuang, Yajie Zhao, Mingming He, Karl Bladin, and Hao Li. Dynamic facial asset and rig generation from a single scan. *ACM Transactions on Graphics (TOG)*, 39(6):215:1–215:18, 2020a.
- Linzhou Li, Yumeng Li, Yanlin Weng, Youyi Zheng, and Kun Zhou. Rgbavatar: Reduced gaussian blendshapes for online modeling of head avatars. In *Computer Vision and Pattern Recognition (CVPR)*, pages 10747–10757, 2025.
- Ruilong Li et al. Learning formation of physically-based face attributes. In *Computer Vision and Pattern Recognition (CVPR)*, 2020b.
- Tianye Li, Timo Bolkart, Michael J Black, Hao Li, and Javier Romero. Learning a model of facial shape and expression from 4d scans. *ACM Transactions on Graphics (TOG)*, 36(6):194:1–194:17, 2017.
- Chen-Hsuan Lin, Jun Gao, Luming Tang, Towaki Takikawa, Xiaohui Zeng, Xun Huang, Karsten Kreis, Sanja Fidler, Ming-Yu Liu, and Tsung-Yi Lin. Magic3d: High-resolution text-to-3d content creation. In *Computer Vision and Pattern Recognition (CVPR)*, 2023.
- Lijuan Liu, Youyi Zheng, Di Tang, Yi Yuan, Changjie Fan, and Kun Zhou. A framework for locally retargeting and rendering facial performance. *Computer Animation and Virtual Worlds (CAVW)*, 22, 2011.
- Ruoshi Liu, Rundi Wu, Basile Van Hoorick, Pavel Tokmakov, Sergey Zakharov, and Carl Vondrick. Zero-1-to-3: Zero-shot one image to 3d object. In *International Conference on Computer Vision (ICCV)*, 2023.
- Zhongjin Luo et al. Rabbit: Parametric modeling of 3d biped cartoon characters with a topological-consistent dataset. In *Computer Vision and Pattern Recognition (CVPR)*, 2023.
- Shengjie Ma, Yanlin Zhao, Hongrui Zheng, Jingxiang Bao, and Yebin Liu. 3d gaussian blendshapes for head avatar animation. In *ACM SIGGRAPH 2024 Conference Proceedings*, 2024.
- Wenchao Ma, Dario Kneubühler, Maurice Chu, Ian Sachs, Haomiao Jiang, and Sharon X Huang. Riganyface: Scaling neural facial mesh auto-rigging with unlabeled data. In *Neural Information Processing Systems (NeurIPS)*, 2025.
- Xuan Ming et al. High-quality mesh blendshape generation from face videos via neural inverse rendering. In *European Conference on Computer Vision (ECCV)*, 2024.
- Jun-yong Noh and Ulrich Neumann. Expression cloning. In *SIGGRAPH*, pages 277–288, 2001.
- Verónica Orvalho, Pedro Bastos, Frederic I Parke, Bruno Oliveira, and Xenxo Alvarez. A facial rigging survey. In *Eurographics State of the Art Reports (EG STAR)*, pages 183–204, 2012.
- Verónica C Orvalho, Ernesto Zacur, and Antonio Susin. Transferring the rig and animations from a character to different face models. *Computer Graphics Forum (CGF)*, 27(8):1997–2012, 2008.

- Pascal Paysan et al. A 3d face model for pose and illumination invariant face recognition. In *Advanced Video and Signal Based Surveillance (AVSS)*, 2009.
- Ben Poole, Ajay Jain, Jonathan T. Barron, and Ben Mildenhall. Dreamfusion: Text-to-3d using 2d diffusion. In *International Conference on Learning Representations (ICLR)*, 2023.
- Shenhan Qian, Tobias Kirschstein, Liam Schoneveld, Davide Davoli, Simon Giebenhain, and Matthias Nießner. Gaussianavatars: Photorealistic head avatars with rigged 3d gaussians. In *Computer Vision and Pattern Recognition (CVPR)*, pages 20299–20309, 2024.
- Dafei Qin, Jun Saito, Noam Aigerman, Thibault Groueix, and Taku Komura. Neural face rigging for animating and retargeting facial meshes in the wild. In *SIGGRAPH*, pages 68:1–68:11, 2023.
- Anurag Ranjan, Timo Bolkart, Soubhik Sanyal, and Michael J Black. Generating 3d faces using convolutional mesh autoencoders. In *European Conference on Computer Vision (ECCV)*, 2018.
- Rakesh Ranjan, Andrea Vedaldi, Mahima Gupta, Christopher Ocampo, and Ocean Quigley. Introducing meta 3d assetgen 2.0: A new foundation model for 3d content creation. <https://developers.meta.com/horizon/blog/worlds/AssetGen2/>, 2025. Accessed: May 22, 2026.
- Nikhila Ravi, Valentin Gabeur, Yuan-Ting Hu, Ronghang Hu, Chaitanya Ryali, Tengyu Ma, Haitham Khedr, Roman Rädle, Chloe Rolland, Laura Gustafson, et al. SAM 2: Segment anything in images and videos. *arXiv preprint arXiv:2408.00714*, 2024.
- Jian Ren et al. Make-a-character: High quality text-to-3d character generation within minutes. *arXiv preprint arXiv:2312.15430*, 2023.
- Disney Research. CANRig: Cross-attention neural face rigging with variable local control. In *SIGGRAPH*, 2026.
- Roger B Ribera et al. Facial retargeting with automatic range of motion alignment. *ACM Transactions on Graphics (TOG)*, 36(4), 2017.
- Nadine Rüegg, Silvia Zuffi, Konrad Schindler, and Michael J Black. BARC: Learning to regress 3d dog shape from images by exploiting breed information. *International Journal of Computer Vision (IJCV)*, 131:3041–3061, 2023.
- Yeongho Seol, Jaewoo Seo, Paul H Kim, J P Lewis, and Junyong Noh. Artist friendly facial animation retargeting. *ACM Transactions on Graphics (TOG)*, 30(6):162, 2011.
- Yeongho Seol et al. Spacetime expression cloning for blendshapes. *ACM Transactions on Graphics (TOG)*, 31(2), 2012.
- Nicholas Sharp, Souhaib Attaiki, Keenan Crane, and Maks Ovsjanikov. Diffusionnet: Discretization agnostic learning on surfaces. *ACM Transactions on Graphics (TOG)*, 41(3):27:1–27:16, 2022.
- Yawar Siddiqui, Tom Monnier, Filippos Kokkinos, Mahendra Kariya, Yanir Kleiman, Emilien Garreau, Oran Gafni, Natalia Neverova, Andrea Vedaldi, Roman Shapovalov, and David Novotny. Meta 3d assetgen: Text-to-mesh generation with high-quality geometry, texture, and pbr materials. *arXiv preprint arXiv:2407.02445*, 2024.
- Olga Sorkine and Marc Alexa. As-rigid-as-possible surface modeling. *Proc. SGP*, pages 109–116, 2007.
- Robert W Sumner and Jovan Popović. Deformation transfer for triangle meshes. *ACM Transactions on Graphics (TOG)*, 23(3):399–405, 2004.
- Jiaxiang Tang et al. Make-it-vivid: Dressing your animatable biped cartoon characters from text. In *Computer Vision and Pattern Recognition (CVPR)*, 2024.
- Daniel Vlasic, Matthew Brand, Hanspeter Pfister, and Jovan Popović. Face transfer with multilinear models. In *SIGGRAPH Courses*, 2006.
- Chao Wang, Yang Liu, Xiaohu Guo, Zichun Zhong, Binh Le, and Zhigang Deng. Spectral animation compression. *Journal of Computer Science and Technology*, 30(3):540–552, 2015.
- Conall Wang, Di Kang, Hao Sun, Shenhan Qian, Simon Giebenhain, and Matthias Nießner. Mega: Hybrid mesh-gaussian head avatar for high-fidelity rendering and head editing. In *Computer Vision and Pattern Recognition (CVPR)*, 2025a.
- Dilin Wang, Hyunyoung Jung, Tom Monnier, Kihyuk Sohn, Chuhang Zou, Xiaoyu Xiang, Yu-Ying Yeh, Di Liu, Zixuan Huang, Thu Nguyen-Phuoc, Yuchen Fan, Sergiu Oprea, Ziyang Wang, Roman Shapovalov, Nikolaos Sarafianos, Thibault Groueix, Antoine Toisoul, Prithviraj Dhar, Xiao Chu, Minghao Chen, Geon Yeong Park, Mahima Gupta,

- Yassir Azziz, Rakesh Ranjan, and Andrea Vedaldi. Worldgen: From text to traversable and interactive 3d worlds. *arXiv preprint arXiv:2511.16825*, 2025b.
- Jiashun Wang, Xueting Li, Sifei Liu, Shalini De Mello, Orazio Gallo, Xiaolong Wang, and Jan Kautz. Zero-shot pose transfer for unrigged stylized 3d characters. In *Computer Vision and Pattern Recognition (CVPR)*, pages 8704–8714, 2023a.
- Jingying Wang, Yilin Qiu, Keyu Chen, Yu Ding, and Ye Pan. Fully automatic blendshape generation for stylized characters. In *IEEE Conference on Virtual Reality and 3D User Interfaces (VR)*, pages 347–355, 2023b.
- Cheng-hsin Wu et al. Multiface: A dataset for neural face rendering. *arXiv preprint arXiv:2207.11243*, 2022.
- Jun Xiang, Xuan Gao, Yudong Zheng, Zerong Zheng, Yinghao Zhao, Chaopeng Han, Jingxiang Cai, Lei Zhu, Dong Xu, Jingyi Yang, and Yebin Liu. Flashavatar: High-fidelity head avatar with efficient gaussian embedding. In *Computer Vision and Pattern Recognition (CVPR)*, pages 9642–9652, 2024.
- Haotian Yang et al. Facescape: a large-scale high quality 3d face dataset and detailed riggable 3d face prediction. In *Computer Vision and Pattern Recognition (CVPR)*, 2020.
- Shurong Yang, Huadong Li, Juhao Wu, Minhao Jing, Linze Li, Renhe Ji, Jiajun Liang, and Haoqiang Fan. Megactor: Harness the power of raw video for vivid portrait animation. *arXiv preprint arXiv:2405.20851*, 2024.
- Changqian Yu, Jingbo Wang, Chao Peng, Changxin Gao, Gang Yu, and Nong Sang. BiSeNet: Bilateral segmentation network for real-time semantic segmentation. In *European Conference on Computer Vision (ECCV)*, pages 325–341, 2018.
- Jiahe Zhang, Zhiyuan Li, Xin Yu, Yifan Xu, and Wangmeng Zuo. Fate: Full-head gaussian avatar with textural editing from monocular video. In *Computer Vision and Pattern Recognition (CVPR)*, 2025.
- Longwen Zhang, Qiwei Qiu, Hongyang Lin, Qixuan Zhang, Cheng Shi, Wei Yang, Ye Shi, Sibe Yang, Lan Xu, and Jingyi Yu. Dreamface: Progressive generation of animatable 3d faces under text guidance. *ACM Transactions on Graphics (TOG)*, 42(4):138:1–138:16, 2023.
- Chun A Zhu and Chris Joslin. Fabrig: A cloth-simulated transferable 3d face parameterization. In *SIGGRAPH Asia*, 2024.
- Hao Zhu et al. Facescape: 3d facial dataset and benchmark for single-view 3d face reconstruction. *IEEE Transactions on Pattern Analysis and Machine Intelligence (TPAMI)*, 2023.
- Wojciech Zielonka, Timo Bolkart, Thabo Beeler, and Andrea Tagliasacchi. Gaussian eigen models for human heads. In *Computer Vision and Pattern Recognition (CVPR)*, 2025.
- Silvia Zuffi, Angjoo Kanazawa, David W Jacobs, and Michael J Black. 3d menagerie: Modeling the 3d shape and pose of animals. In *Computer Vision and Pattern Recognition (CVPR)*, pages 5524–5532, 2017.

Appendix

A Additional Qualitative Results

This appendix provides additional qualitative result grids beyond Figure 5 in the main text. Each grid follows the same controlled layout as the main qualitative figure: the leftmost column shows the original static surface-only asset, the middle columns show generated expression frames from the OmniFaceRig output, and the rightmost column shows a topology-specific mouth-detail close-up with textured rendering and a subtle mesh overlay. These additional results demonstrate robustness across more identities, styles, and topology families.



Figure 8 Additional qualitative OmniFaceRig results (1). Each row shows one input asset and multiple generated expression frames, with a topology-specific mouth-detail close-up highlighting generated inner-mouth geometry and collision-aware mouth deformation.



Figure 9 Additional qualitative OmniFaceRig results (2). Each row shows one input asset and multiple generated expression frames, with a topology-specific mouth-detail close-up highlighting generated inner-mouth geometry and collision-aware mouth deformation.

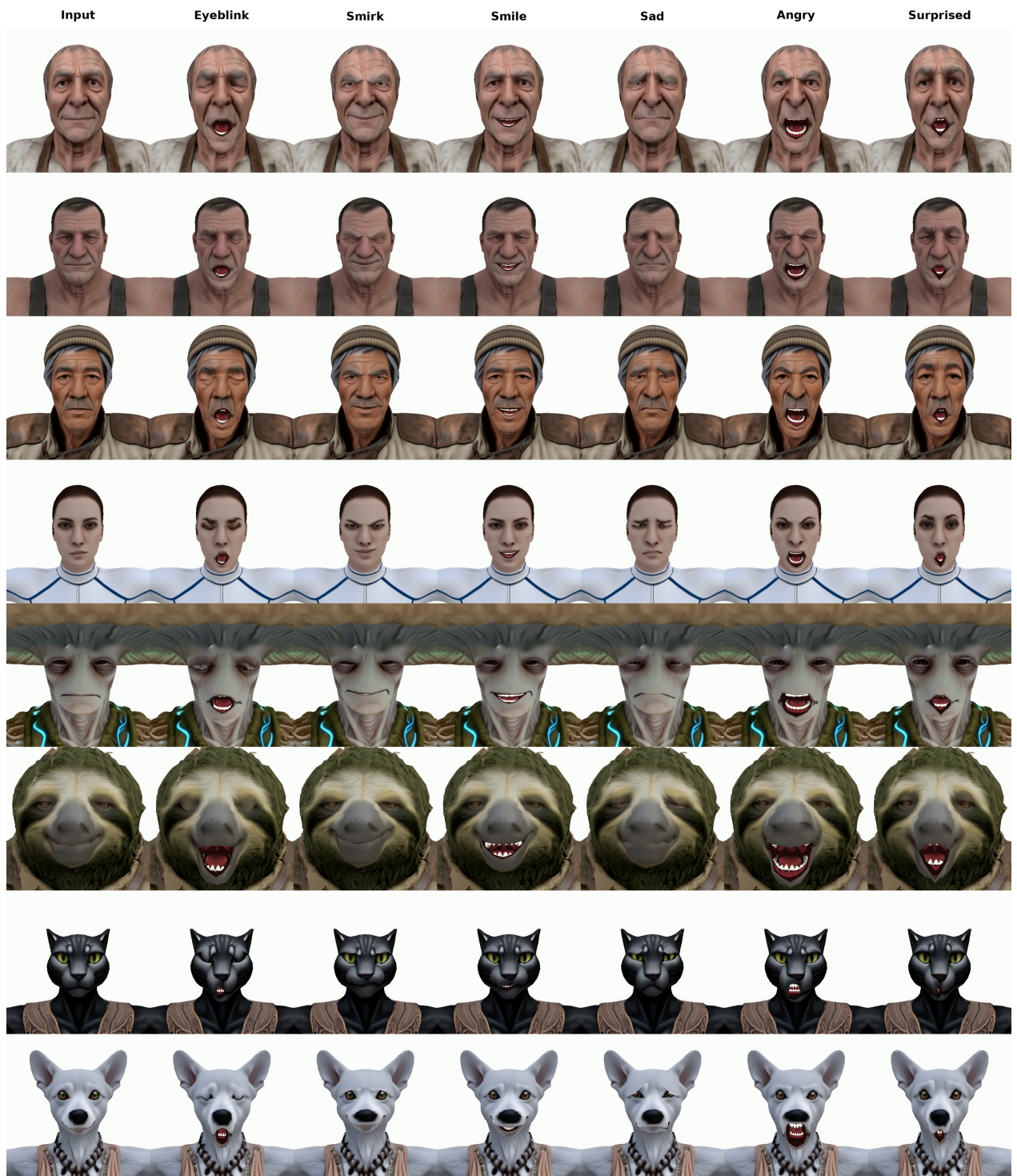


Figure 10 Additional qualitative OmniFaceRig results (3). Each row shows one input asset and multiple generated expression frames, with a topology-specific mouth-detail close-up highlighting generated inner-mouth geometry and collision-aware mouth deformation.



Figure 11 Additional qualitative OmniFaceRig results (4). Each row shows one input asset and multiple generated expression frames, with a topology-specific mouth-detail close-up highlighting generated inner-mouth geometry and collision-aware mouth deformation.

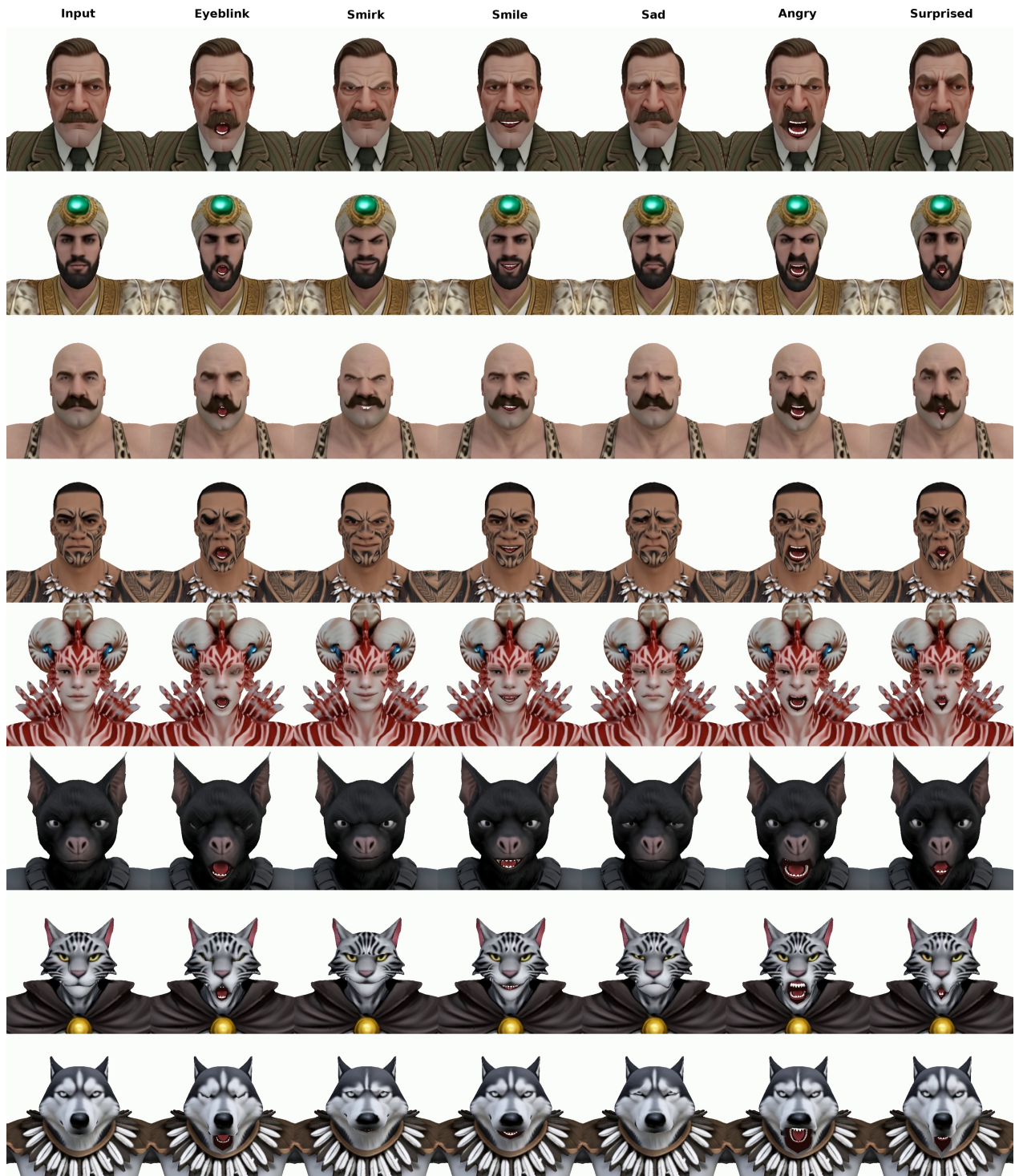


Figure 12 Additional qualitative OmniFaceRig results (5). Each row shows one input asset and multiple generated expression frames, with a topology-specific mouth-detail close-up highlighting generated inner-mouth geometry and collision-aware mouth deformation.

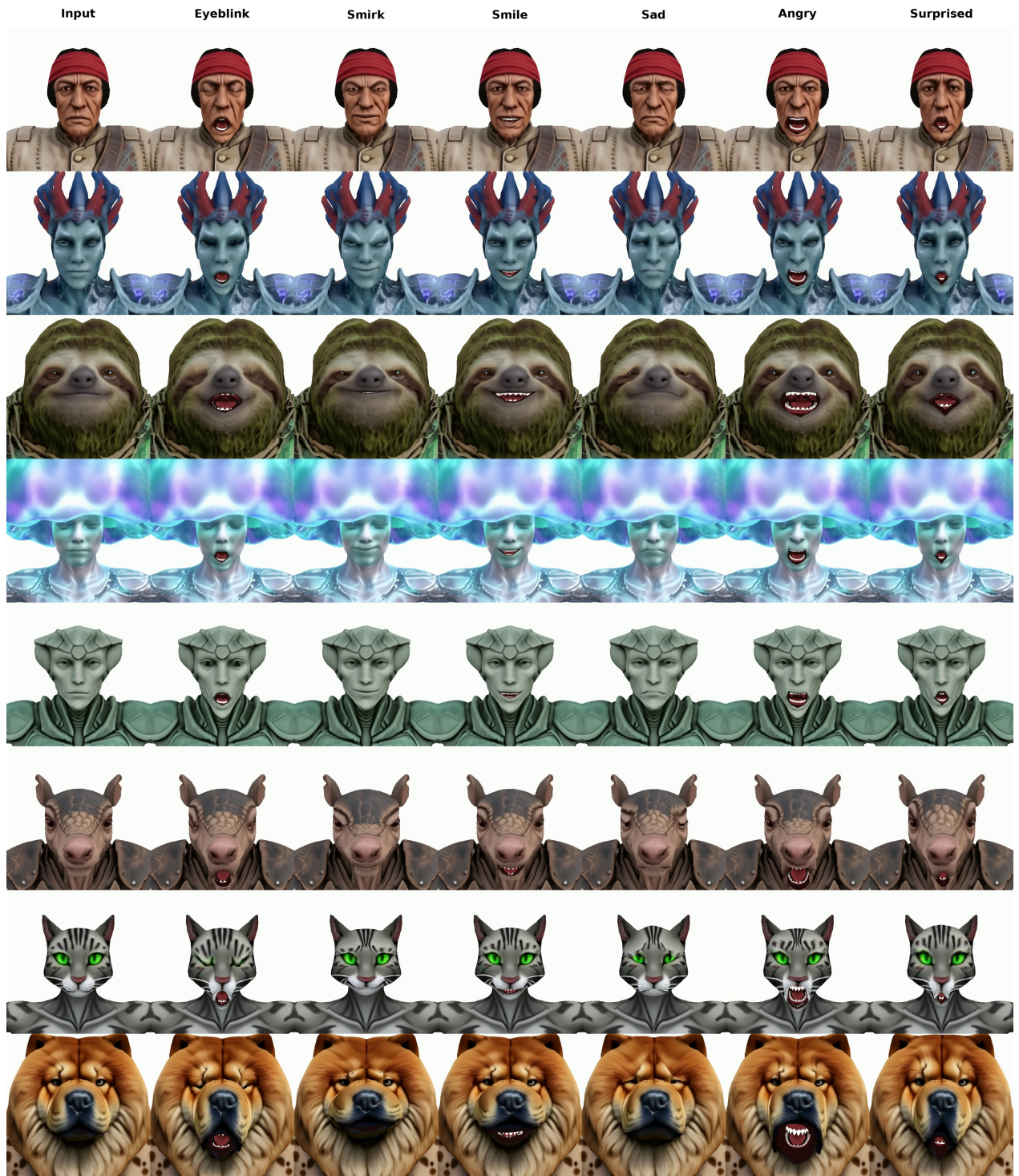


Figure 13 Additional qualitative OmniFaceRig results (6). Each row shows one input asset and multiple generated expression frames, with a topology-specific mouth-detail close-up highlighting generated inner-mouth geometry and collision-aware mouth deformation.



Figure 14 Additional qualitative OmniFaceRig results (7). Each row shows one input asset and multiple generated expression frames, with a topology-specific mouth-detail close-up highlighting generated inner-mouth geometry and collision-aware mouth deformation.